

# Machine learning emulation of precipitation from km-scale regional climate simulations using a diffusion model

Henry Addison<sup>1</sup>, Elizabeth J. Kendon<sup>2,1</sup>, Suman Ravuri<sup>3</sup>, Laurence Aitchison<sup>1</sup>, Peter A.G. Watson<sup>1</sup>

<sup>1</sup>University of Bristol, Bristol, UK

<sup>2</sup>Met Office Hadley Centre, Exeter, UK

<sup>3</sup>NVIDIA Corporation

## Key Points:

- We present a probabilistic machine learning method (CPMGEM) for emulating computationally expensive km-scale regional climate models
- Our emulator of a km-scale UK climate model reproduces well the climatology of daily precipitation conditioned on coarse climate variables
- Our emulator complements the high-resolution climate model with realistic and computationally cheaper samples of daily precipitation

## Abstract

High-resolution climate simulations are valuable for understanding climate change impacts. This has motivated use of regional convection-permitting climate models (CPMs), but these are very computationally expensive. We present a convection-permitting model generative emulator (CPMGEM), to skilfully emulate precipitation simulations by a 2.2km-resolution regional CPM at much lower cost. This utilises a generative machine learning approach, a diffusion model. It takes inputs at the 60km resolution of the driving global climate model and downscales these to 8.8km, with daily-mean time resolution, capturing the effect of convective processes represented in the CPM at these scales. The emulator is trained on simulations over England and Wales from the United Kingdom Climate Projections Local product, covering years between 1980 and 2080 following a high emissions scenario. The output precipitation has a similarly realistic spatial structure and intensity distribution to the CPM simulations. The emulator is stochastic, which improves the realism of samples. We show evidence that the emulator has skill for extreme events with  $\sim 100$  year return times. It captures the main features of the simulated 21st century climate change, but exhibits some error in the magnitude. We demonstrate successful transfer from a “perfect model” training setting to application using GCM variable inputs. We also show that the method can be useful in situations with limited amounts of high-resolution data. Potential applications include producing high-resolution precipitation predictions for large-ensemble climate simulations and producing output based on different GCMs and climate change scenarios to better sample uncertainty.

## Plain Language Summary

Climate models allow us to explore how the climate may change in the future. High-resolution climate models divide the atmosphere into very small boxes (e.g. 2.2 km across). This allows understanding of the changing climate on a local scale, which is important for effective preparation. However, they are slow and expensive to run. This hinders their use for exploring the spread of possible changes at a local scale, particularly for rare events, like heavy rainstorms. We demonstrate a novel use of a generative AI technique to emulate the daily rainfall output of a high-resolution climate model covering England and Wales. That is, to predict the high-resolution daily rainfall when given output from a cheaper, lower-resolution climate model. Our emulator does this faster and more cheaply than the high-resolution climate model and outputs realistic maps of daily rainfall over

England and Wales. It reproduces important statistics of the rainfall distribution from the high-resolution climate model, including examples of the heaviest rainfall events and the main features of the predicted change over the 21st Century. This emulator could be used to produce high-resolution predictions for large sets of coarse climate model output and enable better understanding of potential changes in extreme rainfall.

## 1 Introduction

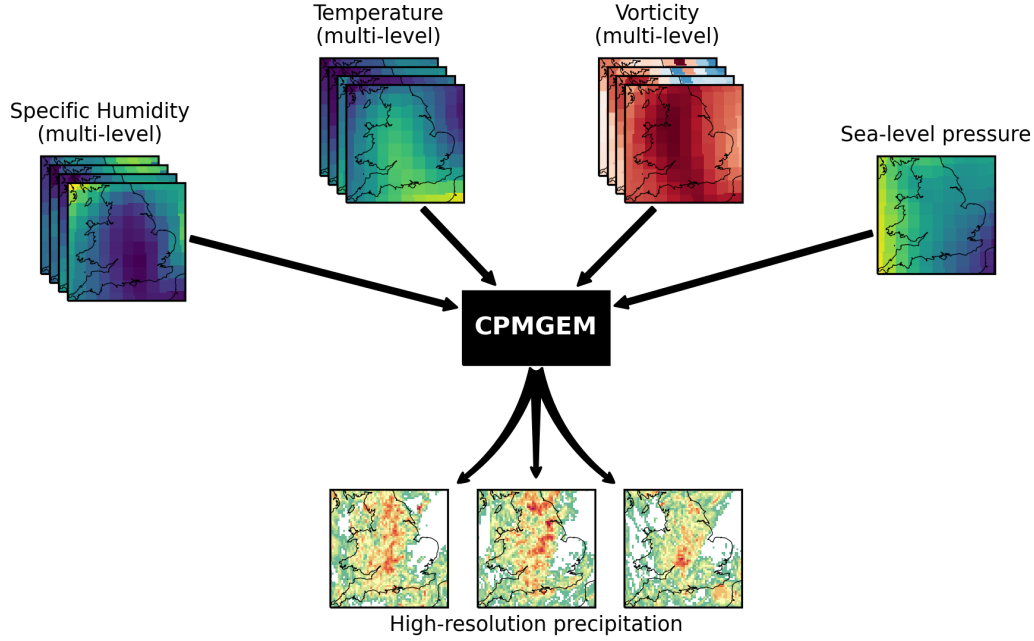


**Figure 1. Schematic diagram of the inputs and outputs of the emulator.** The emulator is trained to stochastically generate samples of high-resolution, daily mean precipitation over England and Wales (bottom panels). The target is for these samples to have properties matching output from the Met Office UK convection-permitting model. The emulator is stochastic, and can generate any number of samples for a single set of inputs. For input fields, the emulator takes variables at the same 60km grid spacing as the global climate model runs used to drive the CPM. These input fields are pressure at mean sea-level and specific humidity, temperature and vorticity at 250, 500, 700 and 850hPa (all daily means).

Understanding precipitation at a local scale is highly important for planning better climate change adaptation measures. Key challenges include representing the fine-scale structure of precipitation and effects such as convection. Convection is a key driver

of many extreme events, but occurs at scales far below the typical resolutions of global climate models (GCMs) (Kendon et al., 2012). This has motivated using regional climate model (RCM) simulations at resolutions high enough to capture these processes, with GCMs providing boundary conditions (e.g., Kendon et al., 2021). These are known as regional convection-permitting models (CPMs). However, running a CPM is very computationally expensive, limiting sampling of climate change scenarios and extreme precipitation events. Furthermore, it is highly technically challenging to run a CPM with output from different GCMs (Sobolowski et al., 2023), limiting exploration of uncertainty in future climate projections at a local scale. Overcoming these challenges would allow for a much more comprehensive understanding of the range of potential severity of future extreme precipitation, for example through studying extreme events with large-ensemble GCM simulations (e.g., Maher et al., 2021; Leach et al., 2022) and covering the range of climate change projections across different GCMs and emissions scenarios (e.g., Eyring et al., 2016).

Here, we demonstrate that a machine learning (ML) emulator of a CPM can produce realistic, high-resolution daily-mean precipitation simulations for England and Wales, conditioned on coarse-resolution weather states produced by a GCM. Our emulator is based on a diffusion model, a state-of-the-art generative ML approach (Sohl-Dickstein et al., 2015; Song et al., 2021). We call it “CPMGEM” (CPM Generative EMulator). A schematic diagram is shown in Figure 1. We trained the emulator using output from the Met Office United Kingdom (UK) CPM, the first set of national-scale CPM climate simulations, which were produced as part of the UK Climate Projections (UKCP) Local product (Kendon et al., 2021, 2023). It produces samples at a small fraction of the computational cost of running a CPM at a resolution that is fine enough to produce information about precipitation at small enough spatial scales for applications such as flood modelling (e.g. Bates et al., 2023). The emulator output is at 8.8km grid spacing, coarser than the 2.2km grid spacing of the CPM, but this reflects the scale of its better-resolved features, which generally span multiple grid boxes (e.g., Klaver et al., 2020).

There exists much previous work on developing statistical methods to predict high-resolution precipitation (e.g., Schoof, 2013; Maraun & Widmann, 2018). However, these methods have generally struggled to produce predictions with realistic spatial structure (Maraun et al., 2019; Widmann et al., 2019), which is important for predicting impacts such as flooding (e.g., Schaller et al., 2020; Archer et al., 2024). One particular challenge

is representing the stochastic aspect of downscaling, where the coarse-scale weather state does not uniquely define the state at a finer scale (e.g., Maraun et al., 2017, 2019). We refer to the difference between the high-resolution precipitation and the best possible deterministic prediction given the coarse inputs as the stochastic component. This component can have a very complex structure at fine scales, particularly when small-scale convection plays a substantial role. This is very difficult to represent with conventional statistical or deterministic ML approaches.

The limitations of conventional statistics have motivated application of ML methods, which have been found to be able to make precipitation predictions with high-quality spatial structures. Some previous work has applied ML to downscale coarse-resolution precipitation predictions to capture high-resolution details (e.g., Vosper et al., 2023; L. Harris et al., 2022; Leinonen et al., 2020; Vandal et al., 2018; Sha et al., 2020). However, a CPM has potential to also improve the coarse-scale structure of precipitation events, particularly when convection plays a large role. Some studies have examined ML methods that do not use coarse-resolution precipitation as an input, learning to make predictions based on other fields that specify the weather state, potentially allowing learning of this large-scale added value. These have primarily focussed on deterministic approaches (e.g., Wang et al., 2023; Doury et al., 2024), but these fail to reproduce realistic, fine scale spatial structures compared to other works that use stochastic models of precipitation (e.g., Vosper et al., 2023; Ravuri et al., 2021; L. Harris et al., 2022; Hess et al., 2022). Recent work has also begun exploring the application of stochastic ML methods to predict precipitation based on non-precipitation predictor variables (Addison et al., 2022; Mardani et al., 2023), the approach we use here.

Whilst many statistical downscaling studies have focused on reproducing properties of observations (e.g., Gutiérrez et al., 2019), there is growing interest in learning to emulate high-resolution numerical models (e.g., Walton et al., 2015; Boé et al., 2022; Doury et al., 2023, 2024; Kendon et al., 2025). The goal is to produce output similar to that of the numerical models at much reduced cost, enabling more complete sampling of climate change uncertainty and internal variability. One key advantage of learning to reproduce the output of high-resolution models is the ability to learn the effects of climate change from a physically-based model. For example, in the UK, this includes complex effects such as summer rainfall becoming more concentrated into shorter, more intense downpours with climate change (Kendon et al., 2014, 2021), which may be difficult to

capture using a method trained on observations alone. Another advantage is having potentially larger datasets, which can help with learning a good representation of extreme events.

We show below that our emulator can predict samples of high-resolution precipitation with realistic spatial structures given coarse weather state information from a GCM, with climatological properties very close to those of the original simulations. A key challenge is representing extreme weather events, which may be anticipated to be especially difficult for ML approaches, and it is unclear how well they generally perform in this respect (Watson, 2022, 2023). We show some evidence that our emulator represents events with intensities up to and including the  $\sim 1$ -in-100 year return level well, which is of the order of event intensities that are typically important in high-stakes applications (e.g. Weaver et al., 2017; Watson, 2022). We also show that the emulator captures most of the CPM’s climate change signal.

To our knowledge, our emulator is the first to be shown to satisfy a number of key requirements for high-resolution climate modelling together: producing output based on convective-scale simulations at a sufficiently fine resolution for impacts modelling, with realistic spatial structure, and performing well at capturing structures and frequencies of extreme events with up to at least 100 year return periods, including when conditioned on GCM output data.

## 2 Materials and methods

### 2.1 Data

CPM data for training and evaluation are taken from the UKCP Local product (Kendon et al., 2023, 2021) and the GCM data is from UKCP18 Global simulations that were used to produce boundary conditions for the CPM (Murphy et al., 2018).

#### 2.1.1 *Target CPM precipitation*

We aim to emulate the daily mean precipitation output over England and Wales from the Met Office UK CPM. This dynamical model has a grid spacing of 2.2km covering the UK. The dynamical downscaling is done in two steps. To provide boundary conditions for the UK CPM, Met Office GCM simulations with 60km grid spacing are first dynamically downscaled using a 12km RCM (Kendon et al., 2021). The domain for

the 12km RCM is the EURO-CORDEX grid (Jacob et al., 2014) which covers Europe and parts of the North Atlantic and North Africa (see <https://cordex.org/domains/cordex-region-euro-cordex/> for full definition). The boundary conditions for the UK CPM are then derived from the RCM simulations. The CPM has a skilful representation of convective processes and captures small-scale rainfall systems that are not resolved in the driving GCM (Kendon et al., 2012, 2014, 2020). Note that our emulator just uses input variables on the scale of the GCM grid to directly emulate the UK CPM, and output from the 12km RCM is not used.

We use data from 12 ensemble members. Each member uses a GCM/RCM pair with unique parameter settings, but an identical CPM, and we treat their outputs as being exchangeable. The simulations follow the Representative Concentration Pathway 8.5 (RCP8.5) climate forcing scenario. We use data from three time periods provided in the initial 2021 release of UKCP Local, which we refer to as “Historic” for 1981–2000, “Present” for 2021–2040 and “Future” for 2061–2080. This gives a total of 720 years of data, which allows development of an emulator that can learn to represent extreme events, and also allows evaluation on such cases.

The simulations use a 360-day year, consisting of twelve 30-day months. Simulations begin on 1st December of a given year, so we take each numbered year to run between 1st December to 30th November (e.g. 1981 means 1st December 1980 to 30th November 1981).

We use daily-mean data from the CPM. For our target high-resolution precipitation, we coarsen the CPM output to 8.8km grid spacing using conservative interpolation and extract the England and Wales domain. The scale of resolved features in dynamical climate models is generally several times the grid box spacing (Klaver et al., 2020), so this coarsening captures the better resolved scales. This coarsening also allows a good trade-off between resolution, domain size and compute requirements. The emulator can run well on commodity hardware such as a 10GB NVIDIA GeForce RTX 2080 Ti graphics processing unit. This precipitation resolution in space and time is superior to that recently used for state-of-the-art UK flood risk modelling (Bates et al., 2023), so it is at a useful scale for climate impacts assessment, while the domain is large enough to visualise features such as fronts and mesoscale convective organisation. There are no clear

barriers to increasing the spatial resolution and domain size given sufficient computing resources.

Climate model output is known to have biases compared to observations. The root mean squared (RMS) relative time-mean bias in precipitation for the Met Office UK CPM over the whole UK land domain was found to be 14.6% in winter and 14.5% in summer when driven by ERA-Interim reanalysis (Dee et al., 2011) (25.7% in winter and 15.6% in summer when driven by the GCM) (Kendon et al., 2021). This is an improvement on the bias for the coarser driving models. For our purposes, successful emulation means recreating CPM behaviour, including biases compared to observations. If appropriate, a user can then apply bias-correction using the same methods as would be applied to CPM output.

### *2.1.2 Coarse predictors*

Ideally we could learn a mapping directly from GCM variables, with 60km grid spacing, to high resolution CPM precipitation. However, synoptic-scale features in a CPM and its driving GCM simulation are not always well-aligned, due to internal variability in the CPM and intermediate RCM (also discussed by Doury et al. (2023)). For example, the GCM may simulate precipitation in the west of the UK whilst it is in the east in the CPM on the same day due to a difference in the exact positioning of a weather front. This means that a mapping directly between GCM and CPM variables is very noisy. Instead, we follow the same approach as Doury et al. (2023) and train using data from the CPM that has been coarsened to the GCM resolution using conservative interpolation (referred to as “cCPM”). This ensures that during training, the weather features in the coarse- and high-resolution data are aligned. Once trained, the emulator can use either coarsened CPM variables or GCM variables as inputs.

We have selected predictors of precipitation based on those that have been found useful in previous statistical downscaling work (e.g., Gutiérrez et al., 2019) and based on the understanding of the physical drivers of precipitation (Chan et al., 2018). We use daily-mean predictor variables, as higher time resolution output is not generally as widely available from GCM simulations. Since we train the emulator using coarsened CPM variables as input with the aim to apply it using GCM variables, it is important to select variables that are represented to a similar degree of realism in the CPM and GCM. It



is also important to select variables where the direction of causal influence is primarily from the variables to the high-resolution precipitation. We avoid using the coarse-resolution precipitation or variables in the boundary layer (below  $\sim 850\text{hPa}$ ) as predictors, since these are not represented sufficiently realistically in the GCM. We tested several choices of coarse-resolution predictor variables during the emulator development. In our final design, we use pressure at mean sea level and three variables on levels in the free troposphere: specific humidity, temperature and relative vorticity of the horizontal wind components. For these multi-level variables, we use a range of pressure levels (250, 500, 700 and 850 hPa), similar to previous works (e.g., Gutiérrez et al., 2019; Doury et al., 2023). We use the vorticity rather than the full wind field because vorticity has been found to be a good predictor of convection (Chan et al., 2018) and the divergent component of the horizontal wind and the vertical wind component may be more strongly affected by feedbacks from convection. Vorticity is calculated from eastward and northward wind components on the coarse 60km grid. The full set of coarse input variables to the emulator are:

- pressure at mean sea level
- specific humidity at 850, 700, 500 and 250 hPa
- vorticity at 850, 700, 500 and 250 hPa
- temperature at 850, 700, 500 and 250 hPa

We use the coarse-resolution predictors across the whole England and Wales domain. Note these are different to the inputs used by the CPM, for which atmospheric GCM data is supplied at the boundary of the intermediate 12km RCM. We describe our method as an “emulator” in the sense that it is developed to predict high-resolution precipitation corresponding to a given GCM simulation that has the same properties as precipitation from the CPM. This approach has the benefit of using the physics embedded in the GCM to predict reasonably realistic weather states at coarse-resolution.

## 2.2 ML Models

### 2.2.1 CPMGEM: Diffusion model-based emulator

Figure 1 shows an overview of the emulator’s inputs, outputs and domain. Inputs and outputs cover the same spatial domain. The inputs are the coarse variables described above. The emulator is stochastic and can generate an arbitrary number of samples of

high-resolution precipitation for given coarse-resolution inputs. This means the emulator can learn to represent the inherent stochastic component of the downscaling task. Ideally, the distribution of these samples matches the distribution of high-resolution precipitation that the CPM would produce over many runs using the same driving GCM data, though we cannot directly test this.

The emulator is a diffusion model based on the work of Song et al. (2021). The training process of a diffusion model proceeds by first adding noise in many steps to target samples (precipitation fields in our case) so that they resemble pure noise after the final step. Then a neural network is trained to assist computing of a process which reverses this noising (again over many steps) and thus can be used to turn pure noise into samples from the target distribution (see Appendix A for a fuller description). For our emulator we use Song et al. (2021)’s sub-Variance-Preserving (“sub-VP”) formulation of the stochastic differential equation (SDE) that defines the noise-adding process in their framework. We use their NCSN++ configuration (an improved version of their original Noise Conditional Score Network) as the backbone neural network. We have adapted it to use conditioning information by creating an input to the network based on the coarsened variables and the target field that is to be denoised. We do this by regridding the coarsened variables to the target grid using a nearest neighbour approach and then stacking these upsampled fields with the target field. We added a final single-channel convolutional layer so that the output (the reduced noised version of our noisy target field in the inputs) matches the size of our target. This final network has  $\sim 63\text{M}$  parameters. We train for 20 epochs on the training dataset, after which further training did not show improvements to the loss computed on the validation set nor to our evaluation metrics computed on samples based on the validation set (see Section 2.3.1 for how data was split into training, validation and test sets). We use the Euler-Maruyama method to solve the reverse SDE for generating samples with the fitted network.

On commodity hardware, a single 10GB NVIDIA GeForce RTX 2080 Ti GPU, training took approximately 41 hours. Each set of 6 samples for a single ensemble member’s portion of the test dataset (9 years) took approximately 5 hours to generate on the same hardware (so approximately 360 hours for 6 sample sets for all 108 years from 12 ensemble members, though this can be easily parallelized across multiple GPUs if available). By comparison, a 20 year simulation of the CPM requires 6 months using several hundred CPUs.

### 2.2.2 Comparison methods

We compare results against a deterministic U-Net (Ronneberger et al., 2015). The U-Net architecture has been shown to perform well in similar climate downscaling settings (e.g., Doury et al., 2023; van der Meer et al., 2023). We use a U-Net based on the original architecture by Ronneberger et al. (2015) with adjustments to match the resolution and number of input and output channels of our dataset (64x64 resolution, 13 input channels, 1 output channel). As with the diffusion emulator, the coarse input variables are regridded to the target grid using a nearest neighbour approach so the input and output resolutions are the same. The network has  $\sim 17$ M parameters. We train for 100 epochs using a mean squared error (MSE) loss function (again when the validation set loss stopped improving; this is a different loss function to that used with the diffusion model, so the number of epochs is not expected to be the same). Whilst performance may be improved by using an alternative loss function (e.g., Doury et al., 2024), the advantages and disadvantages of particular loss functions are not yet fully clear, and an approach has not yet been found that results in a U-Net producing predictions with realistic small-scale structure, one of our primary aims. So we have chosen to focus on the commonly applied MSE loss here. We also considered the larger, enhanced U-Net network architecture within by the diffusion model, but we found no improvement when trained with the deterministic MSE loss.

We also compare emulator predictions with a coarsened version of the CPM precipitation. We coarsen it to 60km grid spacing with conservative interpolation, then project it back to 8.8km resolution with bilinear interpolation. This is not a comparison downscaling method, as we do not use precipitation as a predictor in our emulator. Comparison between this and emulator samples indicates the effect of the emulator adding detail at scales finer than the 60km grid spacing of the predictor variables. Note we do not necessarily expect the emulator outputs to share all the large-scale features as cCPM-Bilinear in individual predictions, as these are not necessarily deterministically predictable from the input variables.

## 2.3 Training

### 2.3.1 *Training, validation and test datasets*

The training dataset was used to fit the model parameter values (including for transforming the variables, described below). Results for different emulator designs (e.g. choices of predictor variables and transformations) were checked on the validation dataset and used to select the final version. All results shown in this manuscript are based on the test dataset, giving an unbiased estimate of the emulator’s quality.

For each 20 year time period, the training dataset includes 14 years in total (70%) and the validation and test datasets include 3 years each (15%). Across all three time periods and 12 ensemble members, this sums to 504 simulated years of training data and 108 simulated years in each of the validation and test datasets. These datasets were constructed by selecting whole seasons (spring, summer, autumn and winter) at random, with an equal number of each season in each dataset. For each selected season we take data from all 12 CPM ensemble members, so that each subset has equal proportions across the ensemble members. Note the GCM ensemble members are independent of each other except for using the same climate forcings, so in a given season the ensemble samples a broad range of weather states. For example, the test dataset is formed of three randomly chosen springs, summers, autumns and winters from each time period (combining data from all 12 ensemble members for the chosen days). Selecting data by season means that we have minimal data leakage between the training, validation and test datasets due to auto-correlation between days, but also means the data in each subset cover a wide range of years and sample a representative set of climatic conditions, following Schultz et al. (2021).

### 2.3.2 *Variable transformations*

We apply transformations to the data to improve the emulator’s performance. To produce target data for training the emulator’s neural network, we first take the square root of the precipitation to produce a less skewed distribution than the raw precipitation, which has many zero values and a long tail. (An alternative approach is a log-based transformation (e.g., L. Harris et al., 2022), but this led to unrealistic samples being output by our diffusion model.) Then we linearly map the square-rooted values so that those in the training dataset lie in the interval  $[-1, 1]$ . This is inverted upon sampling, and any

negative value increased to 0 before squaring (this clipping affects about 15% of values, but in practice all are very small: if they were positive values, they would all correspond to precipitation amounts less than 0.15 mm/day, with 90% of cases under 0.003 mm/day).

Input variables are standardised to have a mean of zero and standard deviation of one (when pooled for all grid boxes, ensemble members and times) in the coarsened CPM training subset.

### 2.3.3 Adjustment of GCM inputs

When using predictor variables from the GCM, it was found to be beneficial to adjust their mean and standard deviation to match those of the coarsened CPM variables, based on the training dataset. This is to account for systematic differences between the GCM and CPM variables at coarse resolution. This was done for each coarse grid box separately. For  $x_g$ , the value of a variable at grid box  $g$ , the adjusted value of the variable,  $\tilde{x}_g$ , is defined as:

$$\tilde{x}_g = \left( \frac{x_g - \bar{x}_g^{GCM}}{s_g^{GCM}} \right) s_g^{CPM} + \bar{x}_g^{CPM} \quad (1)$$

where  $\bar{x}_g^{GCM}$  and  $s_g^{GCM}$  are the mean and standard deviation of the values of  $x$  taken from GCM at grid box  $g$  from the training dataset, and  $\bar{x}_g^{CPM}$  and  $s_g^{CPM}$  are the equivalent for CPM-sourced values of the variable.

The adjusted GCM inputs are then standardised as in Section 2.3.2, based on the mean and standard deviation of the pooled adjusted GCM training dataset. Kendon et al. (2025) discuss further the effects of this adjustment.

## 2.4 Evaluation diagnostics

We test two inference modes of the CPMGEM emulator:

- CPMGEM.cCPM, which uses coarsened CPM variables as inputs, as used in training.
- CPMGEM.GCM, which uses GCM variables as inputs, corresponding to how CPMGEM would be used in practice.

In the coarsened cCPM setting, we make comparisons with the deterministic U-Net emulator, denoted by “U-Net\_cCPM”, and with bilinear interpolation of the coarsened precipitation (denoted “cCPM Bilinear”). For the stochastic CPMGEM emulator, we generated 6 samples for each day in both inference modes.

Below, we describe evaluation diagnostics that require more detailed explanation than can be given in the results section.

#### *2.4.1 Radially Averaged Power Spectral Density*

We use RAPSD to compare the complexity of structures (the variability over different spatial scales) produced by different approaches (D. Harris et al., 2001; Sinclair & Pegram, 2005). To compute the power spectrum of a precipitation field, we compute the 2D Fourier transform of the field and convert to power by multiplying by complex conjugate. We then radially average over nested annuli centred on the origin in the 2D spatial frequency space to create a 1D vector of power at different frequency bands. Finally to compare difference approaches, we compute the mean for each frequency band over all samples.

#### *2.4.2 Spread-Error plot*

To evaluate the size of the stochastic component of the diffusion model emulator, we follow the approach of Leutbecher and Palmer (2008) and produce a spread-error plot, also discussed by Haynes et al. (2023). The idea is that if the CPM simulation output is statistically similar to samples from the emulator for a given GCM state, as in the ideal case, then the relationship with the mean of the samples should be identical for CPM and emulator outputs. Then the root mean square difference between the emulator ensemble mean and the CPM output (the root mean square error, RMSE, of the ensemble mean) and the root mean square difference between the emulator ensemble mean and the individual emulator samples (the root mean square spread, RMSS) should be equal. To account for the finite ensemble size of the emulator output, RMSS has a correction factor of  $\frac{n+1}{n-1}$  applied, where  $n$  is the number of emulator samples generated for each simulator example (in our case,  $n = 6$ ).

This is also the case if samples are binned into intervals of the RMSS. The spread-error plot compares the RMSE and RMSS within these bins, with values calculated for

every grid box and example in the test dataset. We compute the squared spread of emulator samples and squared error for the mean of the samples for each grid box in every example of the test subset. We group these pairs of spread and error into bins containing an equal number of values according to this spread and plot the RMSS and the corresponding RMSE for the predictions in each bin.

### ***2.4.3 Bootstrapping domain mean change confidence intervals***

We use bootstrapping (Efron, 1982) to estimate the sampling variability of the change in seasonal domain mean precipitation going from Historic to Future time periods for our emulator in Section 3.3. In particular, to estimate 95% confidence intervals of the values. For a given season and time period, we sample with replacement from the set of 36 seasonal domain means across the ensemble members and time period (12 ensemble member by 3 years) to produce paired estimates of both the CPM domain mean and emulator domain mean (so sampling the same set of GCM states for each). By repeating this resampling 100,000 times for both time periods we estimate the 0.025 and 0.975 quantiles of the change in the mean from Historic to Future time periods for the CPM and emulator.

## **3 Results**

Below, we present an evaluation of our emulator’s performance at reproducing the UK CPM’s properties. We first test the emulator using CPM data coarsened to the 60km GCM grid as input (CPMGEM\_cCPM), to correspond to the inputs used in training. Our next set of tests use predictors from the GCM (CPMGEM\_GCM) to evaluate how well the emulator transfers to the challenge of predicting high-resolution precipitation when CPM data is not available, including capturing the climate change response. Finally, we evaluate the performance when there is a limited amount of training data.

Some further results are also presented by Kendon et al. (2025), relating to their discussion of methods for emulating regional climate models more generally.

### **3.1 Evaluation using coarsened CPM predictors**

Here, we evaluate our emulator using coarsened CPM data as inputs and compare its predictions with those from the deterministic U-Net (“U-Net\_cCPM”, see Section 2.2.2).

We also compare with bilinear interpolation of the coarsened CPM precipitation (“cCPM Bilinear”), to indicate the difference in spatial detail between GCM and CPM resolutions.

### 3.1.1 *Evaluation on full domain*

We show example predictions of daily mean precipitation in Figure 2. This shows examples on days with substantial precipitation, selected according to the domain-mean value in the CPM. The first row is a wet day in winter, December–February (“DJF Wet”, the 80th percentile across domain means for all winter examples in the test subset). The second row is the wettest winter day (“DJF Wettest”, the winter example from the test set with the maximum domain-mean). The domain-mean precipitation in this example is only expected about once every 108 years, making this a test of the models’ skill for extreme events of intensities relevant to planning climate resilience (Weaver et al., 2017; Watson, 2022). The third and fourth rows are similar but for summer, June–August (“JJA Wet” and “JJA Wettest”). Here, “JJA Wet” is an example chosen to have precipitation close to the 80th percentile and also a large region of convective showers, to illustrate the performance for this weather type. The other three examples show precipitation patterns characteristic of fronts.

The first column is the target CPM precipitation. The second column shows results from bilinear interpolation of coarsened CPM precipitation (cCPM Bilinear). The third column is vorticity at 850hPa derived from coarsened wind fields from the CPM. It is an example of the coarse inputs used by the emulator and provides a visualization of one of the features it sees.

The fourth and fifth columns show two samples from the diffusion model (randomly chosen from the six). These demonstrate the emulator’s ability to produce daily-mean precipitation samples with realistic fine detail. For DJF Wet it recreates the high intensity structures in the southern half of the domain whilst also having realistic lower intensity showers further north. For JJA Wet, it predicts small clusters of high intensity, similar to those seen in the CPM output. The predictions for the extreme examples in the second and fourth rows also have similarly realistic spatial structure to the CPM. Note, there is a substantial stochastic component of precipitation that is unpredictable given just the coarse-scale state and selecting the most extreme day in CPM output will



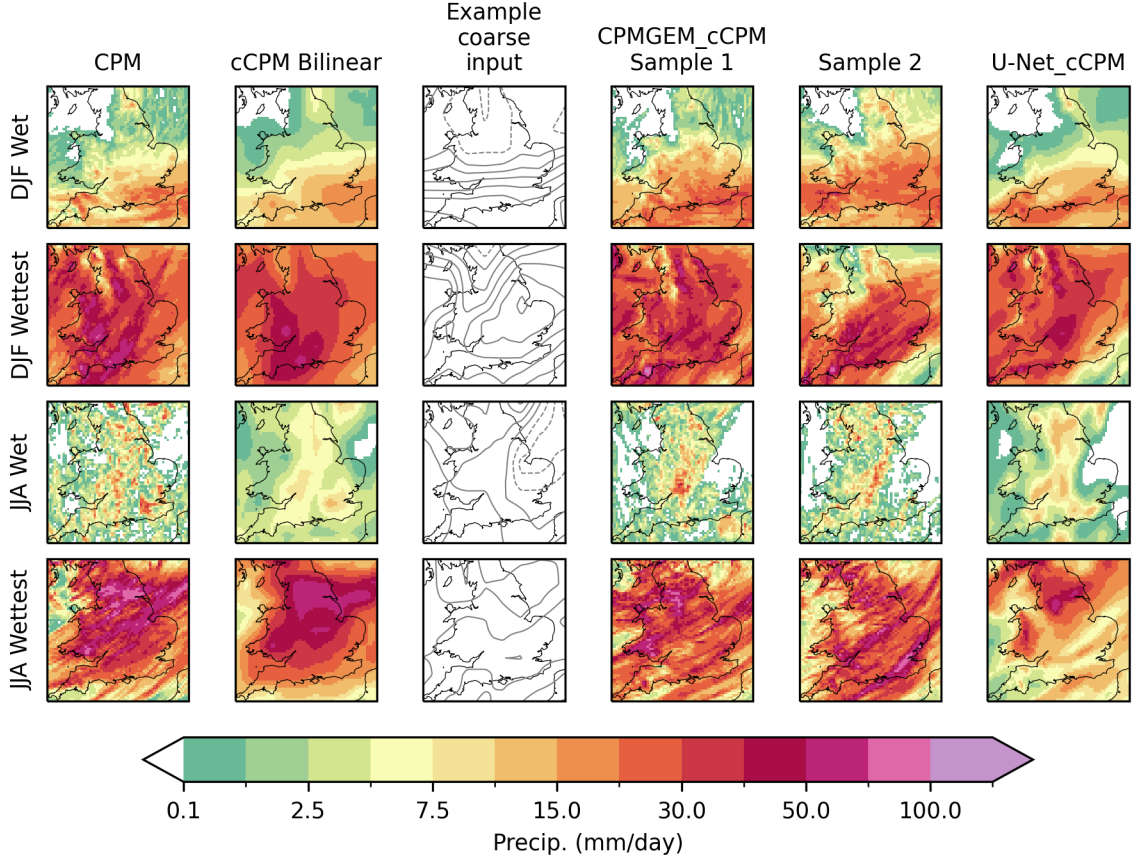


**Figure 2. Examples of predictions of daily-mean precipitation.** The first row shows results for a wet day in winter (December–February, DJF; the 80th percentile of the domain-mean). The second row shows the wettest winter day in the 108 year test dataset. The third and fourth rows are similar but for summer (June–August, JJA). The first column is the precipitation from the convection-permitting model (CPM). The second column is the coarsened CPM precipitation bilinearly interpolated to 8.8km resolution of our emulator. Column 3 is an example coarse resolution input field, the 850hPa vorticity. Contours, in grey, are drawn in steps of  $2 \times 10^{-5} \text{s}^{-1}$  between  $-10^{-4} \text{s}^{-1}$  and  $+10^{-4} \text{s}^{-1}$  with dashed lines for negative values and solid lines for positive. Columns 4 and 5 are samples chosen at random from the emulator using coarsened CPM atmospheric variables as predictors (CPMGEM\_cCPM). Column 6 is the prediction by U-Net. Note that the highly stochastic nature of precipitation downscaling means samples from the diffusion model are not expected to match the CPM precipitation in full detail, but to represent the distribution of plausible precipitation fields for the given low resolution predictors, where the CPM simulation output is a single example.

tend to select a day when this component is positive and relatively large. Therefore it would not necessarily be expected that typical samples from the emulator for the same day would reach as intense values as in the CPM. (Evaluation of the overall intensity distribution across all days, including whether the emulator accurately reproduces the frequency of extreme values, is presented later in this section.)

The rightmost column shows predictions from the deterministic U-Net\_cCPM. While it also mostly correctly represents the large-scale patterns (like the fronts in rows 2 and 4), it does not recreate the fine level detail of the CPM simulations. This is similar to other deterministic downscaling models (e.g., Doury et al., 2024; Sha et al., 2020). This is very noticeable in the JJA Wet case, for which it predicts a much smoother rainfall field, with lower peak intensity than seen in either the CPM or CPMGEM\_cCPM.

The differences between the two CPMGEM\_cCPM samples indicate the size of the stochastic component as learnt by the emulator. Whilst the large-scale features are fairly similar, as expected since the samples are conditioned on the same coarse-scale input, the locations of the heaviest precipitation amounts generally differ, which may result in very different local effects simulated by an impacts model. This indicates that the stochastic component is generally large and it is important that it is represented. The CPMGEM\_cCPM samples also illustrate how the emulator could generate different realisations of a given day’s precipitation, perhaps to explore the impact if the heaviest downpours occurred in different locations, for example in areas with critical infrastructure. (This could be an interesting application of a similar emulator trained on observations and applied to historical weather events, although we do not explore this here.)

As well as producing realistic samples, it is important that the frequency distribution of precipitation produced by the emulator matches that of the CPM. Figure 3(a) shows the frequency distribution of precipitation across all 8.8km grid boxes for the CPM, the downscaling models and the results of cCPM Bilinear. The distribution of CPMGEM\_cCPM matches that of the CPM distribution very closely up to intensities of over 200 mm/day, the extreme tail of the test set (there are only two CPM simulated values beyond the maximum shown). Note the log scale of the density axis.

Both U-Net\_cCPM and cCPM Bilinear have too low frequencies of precipitation more intense than  $\sim 30$  mm/day. Potentially for U-Net\_cCPM, this could be improved by using a loss function designed to increase prediction of extreme values (e.g., Doury

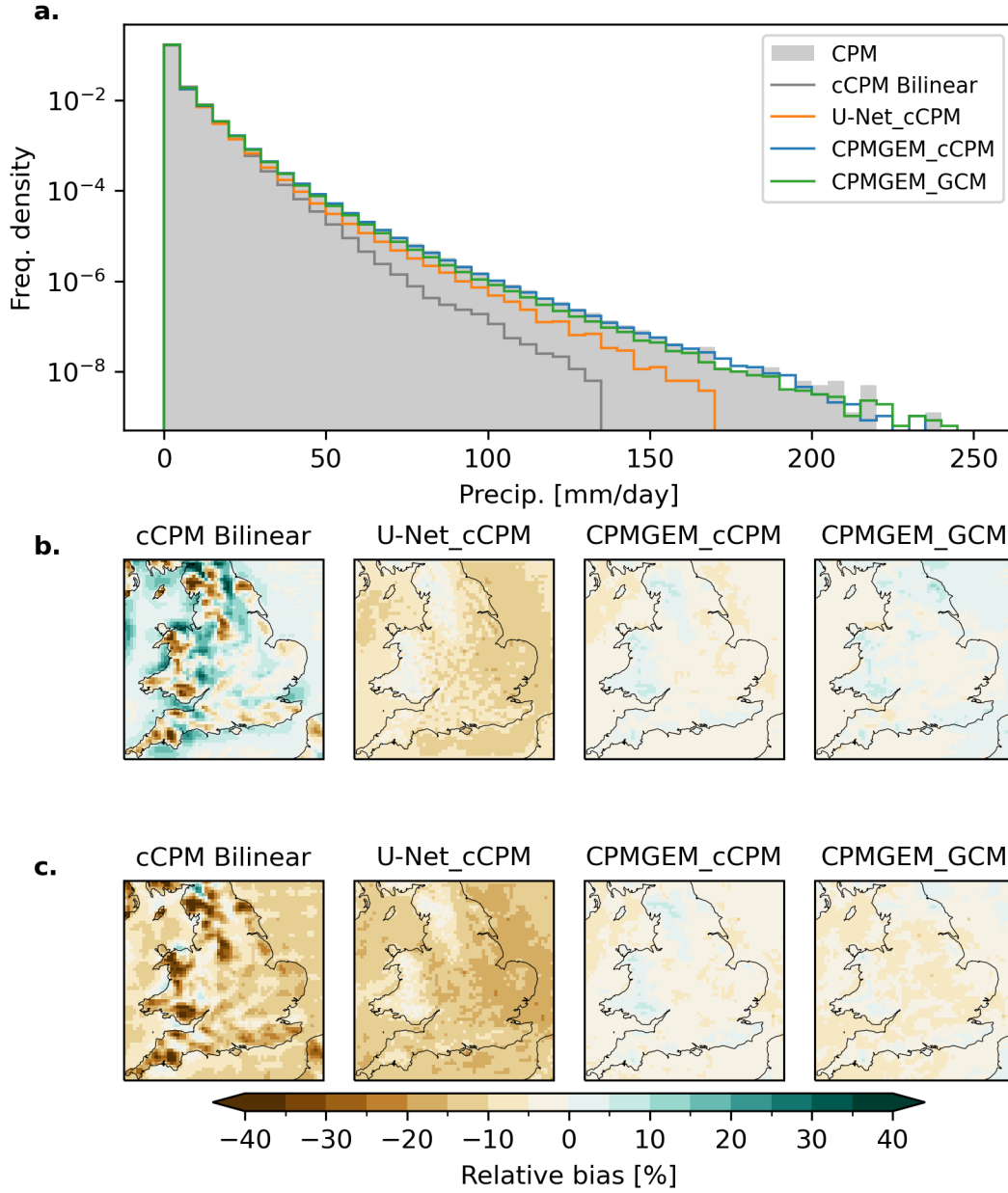


**Figure 3. Statistical properties of predictions.** (a) Histograms of precipitation values on the 8.8km grid. The grey shaded area is the frequency density of the target CPM precipitation. The lines show frequency densities from the diffusion model emulator acting on coarsened CPM and GCM inputs respectively (“CPMGEM\_cCPM” (blue) and “CPMGEM\_GCM” (green)), U-Net\_cCPM (orange) and CPM precipitation coarsened to 60km resolution with bilinear interpolation (cCPM Bilinear; dark grey). Note the vertical axis is logarithmic. (b) Relative mean bias as a percentage of the CPM mean for each model. (c) Same as (b) but for standard deviation bias.

Model	RMS Relative Mean Bias (%)	RMS Relative Std Dev Bias (%)
CPMGEM_cCPM	3.4	3.6
CPMGEM_GCM	2.6	4.6
U-Net_cCPM	9.3	13.3
cCPM Bilinear	10.4	13.8

**Table 1. Root mean square of relative biases.** Computed across the 8.8km output grid boxes for the mean and standard deviation, as plotted in Figure 3(b,c).

et al., 2024). However, it would also be expected that the stochastic aspect of CPMGEM\_cCPM contributes to generating a more accurate frequency of extreme values.

Importantly, the CPMGEM\_cCPM emulator also predicts a similar frequency of wet days as the CPM. The frequency of days with more than 0.1mm of precipitation in individual 8.8km grid boxes is 52.6% for CPMGEM\_cCPM versus 53.0% for the CPM (66.4% versus 67.4% in winter and 36.9% for both cases in summer).

The precipitation distribution varies across the UK, due to effects such as elevation. Figure 3(b) and (c) show spatial maps of the biases in the mean and standard deviation. CPMGEM\_cCPM displays small biases over the whole domain. U-Net\_cCPM has a consistent dry mean bias everywhere and a too low standard deviation (similar to findings of Doury et al. (2024) when using MSE loss), again indicating the likely role of the stochastic part of the precipitation variability in the diffusion model emulator. The cCPM Bilinear biases are substantial in areas with high terrain, such as in northwest and southwest England and in Wales, where there is high spatial variance. The comparison with CPMGEM\_cCPM shows that the emulator has learnt the differences in precipitation properties between nearby locations, below the scale of the coarse-resolution inputs. Table 1 summarises the root mean squares of these biases over space, quantifying the typical sizes of these biases. The mean biases of CPMGEM\_cCPM relative to the CPM are much smaller than the mean bias of the CPM relative to observations (see Section 2.1.1).

As well as matching the climatological distribution of CPM precipitation, the emulator must also learn the dependence of the precipitation distribution on the coarse input variables. We examine this using a scatter plot of domain-mean precipitation from CPMGEM\_cCPM against that from the CPM target (Figure 4(a)). We use the domain-

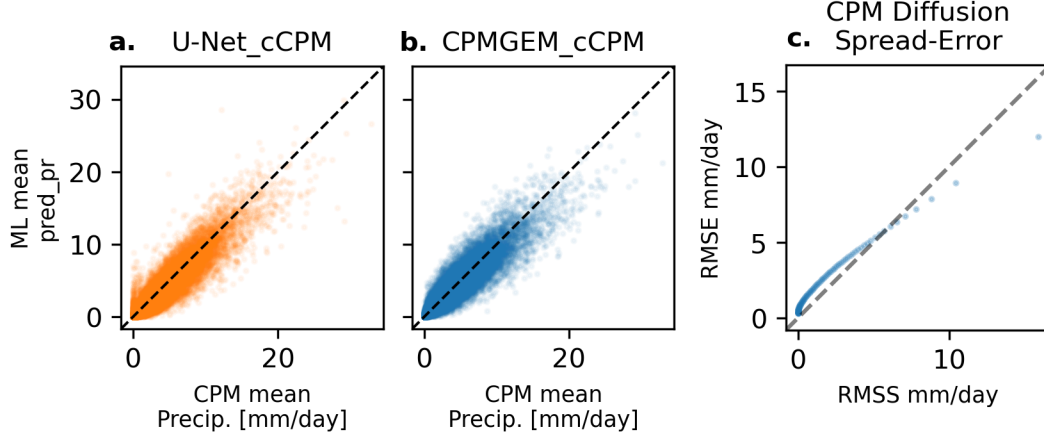


**Figure 4. Spread of predictions.** (a) Scatter plot of daily domain-mean precipitation for samples from CPMGEM\_cCPM versus target CPM values. (b) Same as (a) for U-Net\_cCPM. (c) Spread-error plot of CPMGEM\_cCPM, indicating the calibration of the stochastic component (see Section 2.4.2 for details).

mean because this reduces the variability from the stochastic component sufficiently to be able to clearly see that the predicted and target precipitation are well-correlated. Note that since precipitation likely has a substantial component that is effectively stochastic and unpredictable given only coarse-scale variables, a perfect correlation could not be expected. The degree of correlation is similar for U-Net\_cCPM (Figure 4(b)). This indicates that the deterministic component of CPMGEM\_cCPM (identified conceptually with the mean over many samples) is similarly skilful to predictions from U-Net. Both appear to learn a skilful relationship between the inputs and total precipitation. The stochasticity in the CPMGEM\_cCPM output likely contributes to its predictions having slightly more spread.

It is also important to evaluate whether the size of the stochastic component of the diffusion model emulator is appropriate. Following the approach of Leutbecher and Palmer (2008), we produce a spread-error plot (see Section 2.4.2 for more details). Figure 4(c) shows the root mean square error (RMSE) versus the root mean square spread (RMSS) for samples binned according to the spread of the prediction ensemble for CPMGEM\_cCPM. Ideally, these should be equal for all bins of prediction spread values, taking into account adjustments for having a finite ensemble size. This is approximately the case for CPMGEM\_cCPM across most of the range of spread values, indicating that the stochastic component of

the predictions has an appropriate size, and that the model can skilfully differentiate between situations that are relatively predictable (low spread and error) and less predictable (high spread and error). There is a slight tendency for the emulator to be overconfident for cases with lower spread and to be more noticeably under-confident for cases with higher spread.

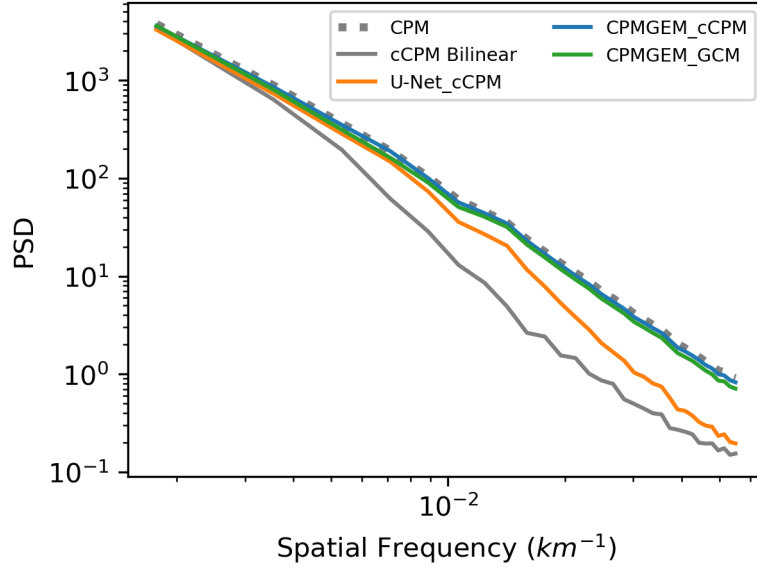


**Figure 5. Radially averaged spatial power spectral density (RAPSD).** Shows the target CPM precipitation (grey dashes), the emulator samples, CPMGEM\_cCPM (blue line) and CPMGEM\_GCM (green line), U-Net\_cCPM (orange) and cCPM Bilinear (dark grey).

To quantitatively evaluate the realism of the spatial structures in the emulator output, Figure 5 shows the radially averaged power spectral density (RAPSD; see Section 2.4.1 for more detail). This quantifies the amount of variance across the range of spatial scales in the data. The RAPSD of the CPM and CPMGEM\_cCPM match closely for the full frequency domain, showing that CPMGEM\_cCPM produces structures which have similar variability at different spatial scales to the CPM simulation. The close agreement at small spatial scales (high frequencies) reflects how the CPMGEM\_cCPM samples include a realistic degree of fine-scale structure, as seen in the samples in Figure 2. The curves for U-Net and cCPM-Bilinear generally display too low variability, particularly at the highest frequencies, corresponding to these predictions having unrealistically smooth small-scale structure, though comparing with cCPM Bilinear indicates that U-Net does

appear to add some variability below the scale of the coarse grid of the input data. Comparing the results for the diffusion model and U-Net indicates that including a stochastic component in the emulator samples has helped to realistically represent small-scale variability.

### 3.1.2 Regions, seasons and different precipitation types

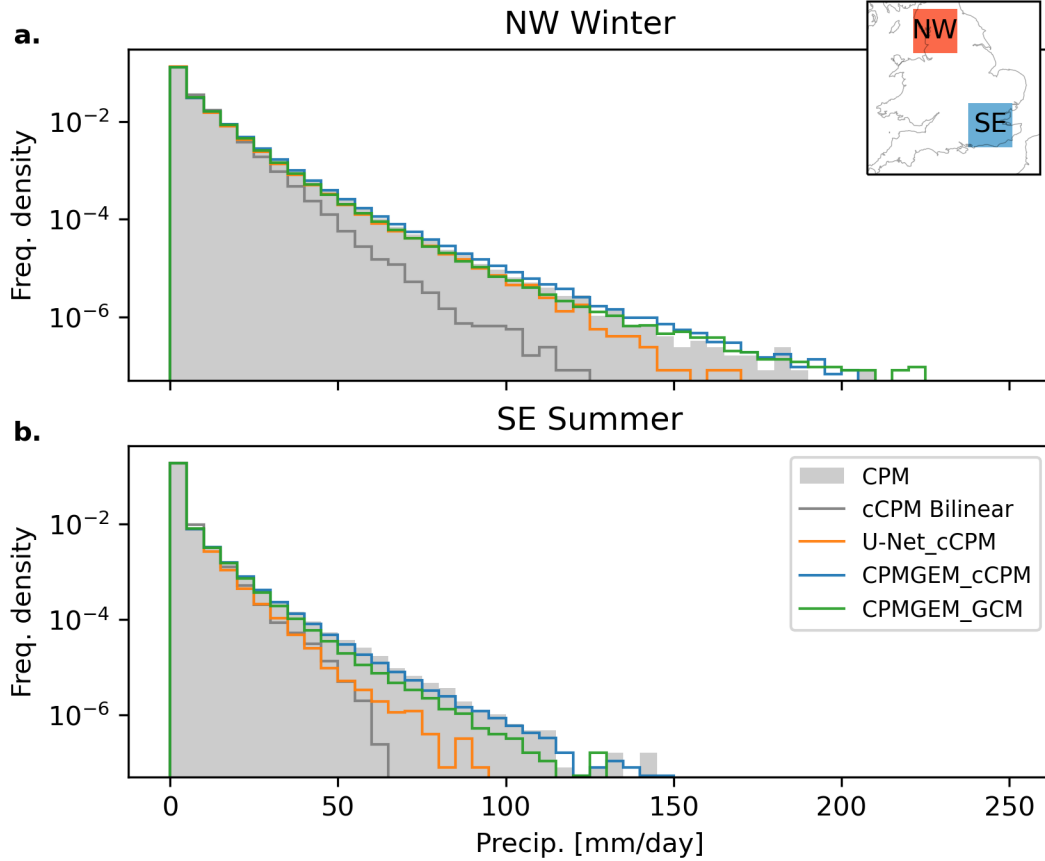


**Figure 6.** Frequency distributions in different regions and seasons. (a) Winter in northwest England, where precipitation is predominantly frontal and orographic; (b) summer in southeast England, which includes a substantial convective precipitation component. Plotted as in Figure 3(a). The inset at the top right shows the regions in the context of the full spatial domain.

Different processes drive UK precipitation to different extents depending on the region and time of year. Therefore we evaluate whether the emulator reproduces these differing regional and seasonal characteristics of precipitation. Figure 6 shows frequency

distributions for precipitation in northwest England in winter and in the southeast in summer across individual points on the high-resolution grid. In the former case, precipitation is predominantly frontal and orographic, while the latter case has a larger convective component. Both regions are  $16 \times 16$  8.8km grid boxes in size.

The frequency distribution of CPMGEM\_cCPM samples closely follows that of CPM precipitation for both cases. The same is not true of samples from U-Net\_cCPM, which matches the northwest winter distribution well until about 125 mm/day, but substantially underpredicts the frequency of more extreme intensities, as for the full frequency distribution shown in Figure 3(a). The agreement between the target CPM and U-Net\_cCPM is closer than for the full distribution, suggesting that the deterministic component of precipitation in this region and season accounts for a larger share of variability, perhaps due to the strong orographic component and importance of large-scale frontal systems, with the stochastic component being more apparent in the most intense extremes. cCPM Bilinear produces a large underestimate for frequencies greater than about 25 mm/day, indicating the relevance of small-scale variability. In the southeast in summer, both U-Net\_cCPM and cCPM Bilinear similarly underestimate the frequency of heavy precipitation. This indicates an important role for the stochastic component of precipitation here, which may be expected given the larger influence of small-scale convective rainfall systems than in the northwest winter case, as in the example in the third row in Figure 2.

### 3.2 Transfer to using GCM inputs

Next we examine how well our emulator transfers to the problem of downscaling GCM data, rather than the coarsened CPM data like that used for training. Having shown the greater realism of CPMGEM outputs compared to U-Net when using coarsened CPM variable inputs above, we focus here just on the performance of the CPMGEM\_GCM emulator.

Figure 7 shows example predictions from the CPMGEM\_GCM model. The GCM-sourced predictors have been adjusted to match the overall mean and variance of cCPM predictors at each location, as described in Section 2.3.3. The rows each correspond to a different day and are chosen in a similar way as in Figure 2, but based on GCM precipitation, with “DJF Wet” and “JJA Wet” days corresponding to the 80th percentile



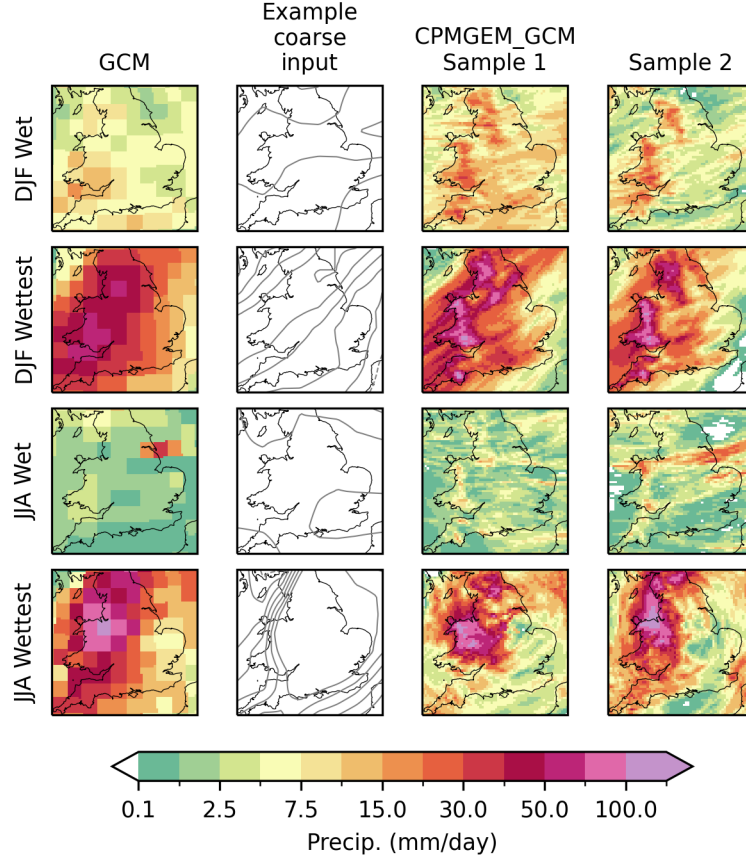


**Figure 7. Samples based on GCM input variables.** Each row shows results for one example day, chosen in a similar way to those in Figure 2, based on domain-mean GCM precipitation. The first column shows the GCM precipitation, the second an example coarse input field (vorticity at 850hPa, contours in grey every  $2 \times 10^{-5} \text{s}^{-1}$  between  $-10^{-4} \text{s}^{-1}$  and  $+10^{-4} \text{s}^{-1}$ , with dashed lines for negative values) and columns 3 and 4 are two samples from the emulator using GCM inputs (CPMGEM\_GCM). Note the emulator output is not constrained to match the coarse-resolution structures of the GCM precipitation, and may predict more realistic features at large as well as small scales.

of the domain-mean, and the other two rows to the wettest winter or summer day in the test subset respectively. The first two columns show data from the GCM for context: the low resolution precipitation and one input to the emulator, the coarsened vorticity at 850hPa. The third and fourth columns show two samples from CPMGEM\_GCM for the given predictor variables. It can be seen that they contain finer spatial detail. Also they do not in general have exactly the same coarse-scale spatial structure as the GCM simulation, as they have learnt a separate model of precipitation based on the CPM target, and so do more than just add spatial detail to the precipitation. For example, the CPMGEM\_GCM samples exhibit heavier precipitation in the western UK in the “DJF Wet” case, which may be associated with the GCM not resolving orography well there. And they show lighter precipitation in southwest England in the “JJA Wettest” case.

Figure 3(a) shows that when working on GCM-derived inputs the emulator (CPMGEM\_GCM) continues to produce samples whose distribution of intensities is still very similar to the CPM precipitation target on the 8.8km grid. It also predicts a similar proportion of wet days (greater than 0.1 mm/day) to the CPM across all grid boxes: 54.7% annually from the emulator compared to 53.0% from the CPM. Seasonal differences in this proportion are also captured by the emulator: 68.1% compared to 67.4% in winter and 38.4% compared to 36.9% in summer. The biases in the mean and standard deviation of precipitation of CPMGEM\_GCM are small relative to the CPM target throughout the spatial domain (Figure 3(b) and (c) and Table 1) and the spatial power spectral density for CPMGEM\_GCM is very similar to CPMGEM\_cCPM and the CPM as well (Figure 5). For the northwest winter and southeast summer (Figure 6), the frequency distributions of precipitation are also very similar, albeit with a slight underestimation of the frequency of days with more than 50 mm/day in the southeast in summer. This indicates that the emulator produces precipitation samples with realistic structures and intensities when given bias-corrected GCM variables as input. Without this adjustment, the emulator had a modest dry bias across the whole domain—results demonstrating this are included in (Kendon et al., 2025).

To indicate how much closer the emulated precipitation is to the CPM output than the GCM precipitation, Figure 8 compares statistics of precipitation on the GCM’s coarse grid between the GCM output and conservatively regridded CPMGEM\_GCM and CPM output. The emulator produces a similar distribution of intensities to the CPM at this coarser scale right up to around the maximum coarsened CPM value from the test set,

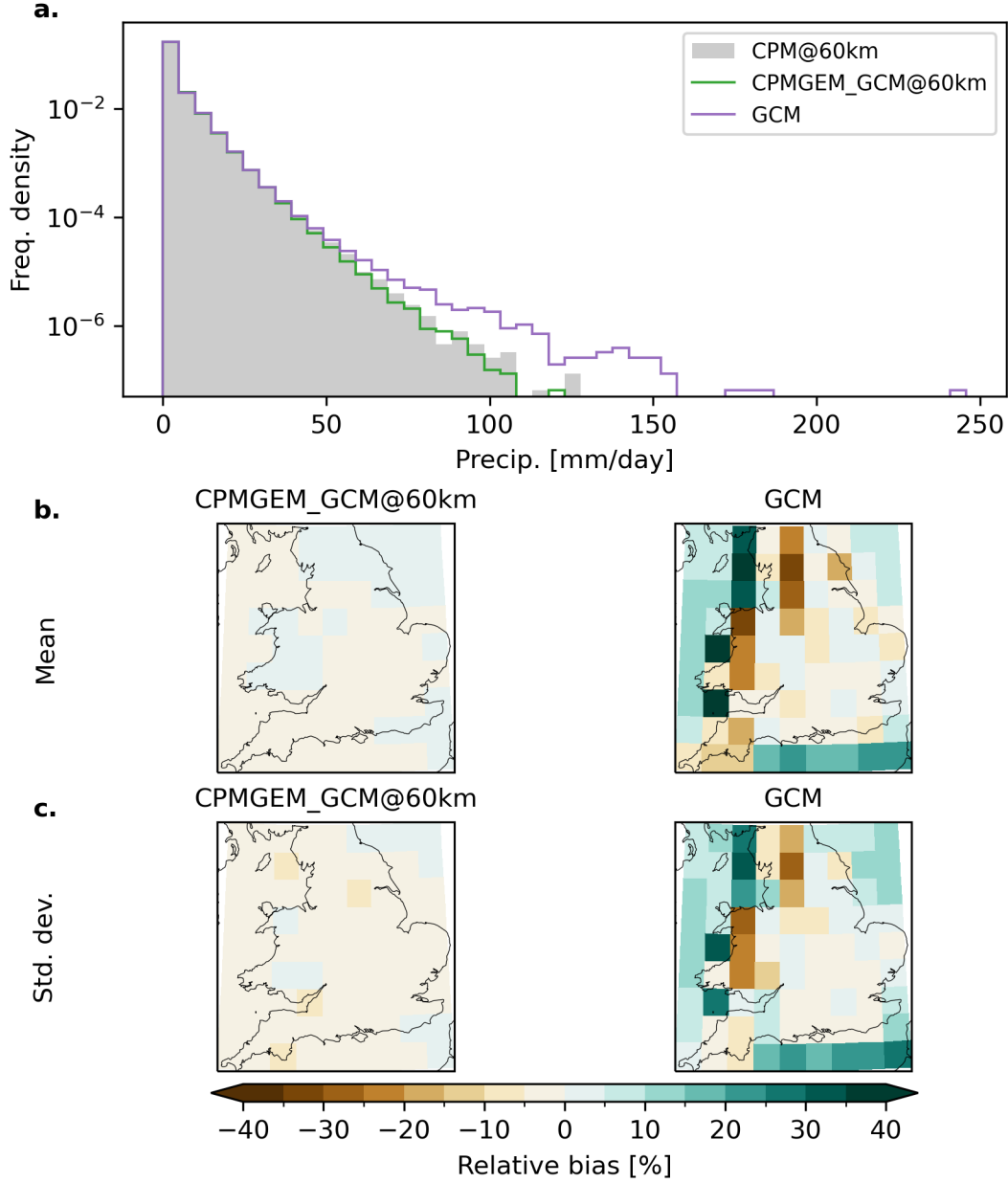


**Figure 8. Statistical comparison with GCM output.** (a) Histograms of daily precipitation values on the 60km grid, for the coarsened target CPM precipitation (grey filled area), the coarsened output of the CPMGEM\_GCM emulator (green), and GCM precipitation (magenta). Note the vertical axis is logarithmic. (b) Relative bias in mean precipitation compared to the CPM for CPMGEM\_GCM (left) and GCM (right) on the coarse grid (in contrast to results shown for precipitation on the fine grid in Figure 3(b)). (c) Same as (b) but for standard deviation bias.

Season	CPM (%)	Emulator (%)	Difference (% of CPM change)	Difference (% of Historic CPM)
Winter	23	17	-26 ( -41 to -10)	-5.9 (-9.5 to -2.3)
Spring	6	2	-61 (-134 to +13)	-3.8 (-8.3 to +0.8)
Summer	-40	-39	2 ( -14 to +18)	0.8 (-5.7 to +7.1)
Autumn	-4	-8	-114 (-240 to +13)	-4.5 (-9.4 to +0.5)

**Table 2. Climate change in the seasonal domain mean.** Changes from Historic to Future periods are shown for each season. The second and third columns contain the relative changes for the CPM and the CPMGEM\_GCM emulator respectively (relative to CPM Historic seasonal domain mean in both cases). The fourth column contains the difference between the change in the CPM and in CPMGEM\_GCM, relative to the change in CPM. The fifth column shows the same difference but relative to the Historic CPM seasonal domain mean. The values in brackets in the fourth and fifth columns are the bootstrapped 95% confidence intervals of the difference.

about 120 mm/day (panel (a)). The distribution of GCM precipitation, however, has an exaggerated tail for values larger than about 50 mm/day. The biases in the mean and standard deviation are much smaller for the emulator than for the GCM, particularly in grid boxes covering upland areas, on parts of the western coast and in the English Channel (Figure 8(b) and (c)).

### 3.3 Climate change comparison

As mentioned in the introduction, a key advantage of training on high-resolution simulation data is the potential ability to learn a physically-based future climate change signal. Figure 9 shows the emulator’s ability to capture the effect of climate change on the precipitation frequency distribution, including extremes. Panel (a) shows the differences in the frequency distribution of precipitation from our emulator (CPMGEM\_GCM) for the three time periods (“Historic” for 1981–2000, “Present” for 2021–2040 and “Future” for 2061–2080). There is an increase in intensities in the tail of the emulator’s distribution as time increases. The other three panels compare distributions from CPMGEM\_GCM, the CPM target and the CPM in the Historic period. The emulator captures the shift away from the Historic distribution over time, as seen particularly clearly in the Future period. However, the increase in intensities is modestly underestimated.

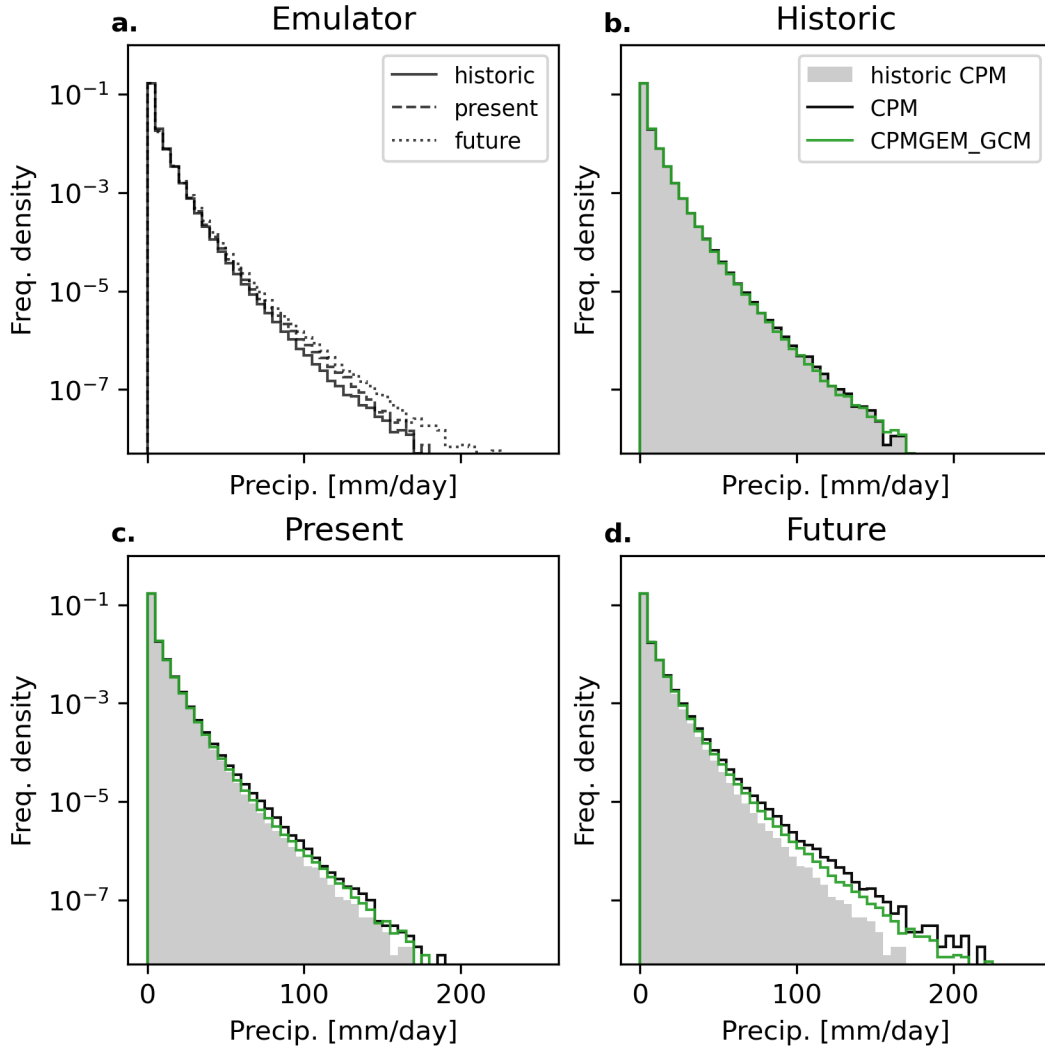


**Figure 9. Climate change effect on precipitation frequency distributions.** (a) shows the different CPMGEM\_GCM frequency densities for the three different time periods: Historic (solid black), Present (dashed black) and Future (dotted black). (b) shows a comparison of the frequency density histogram of CPMGEM\_GCM (green) with the CPM (black) for the Historic time period. (c) and (d) show the same as (b) but for Present and Future time periods respectively. In (b), (c) and (d) the filled grey histogram shows the CPM precipitation frequency distribution from the Historic time period to highlight the change in the precipitation distribution between the time periods.

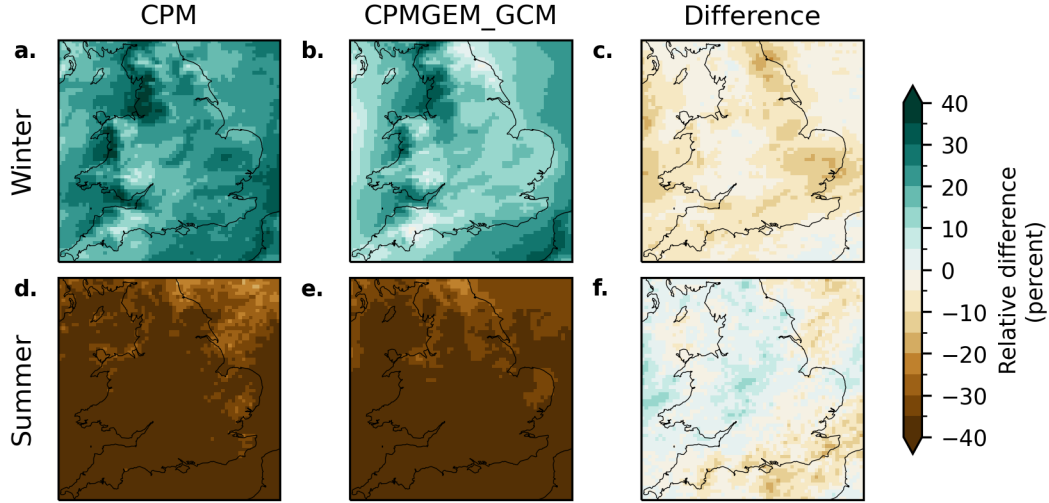


**Figure 10.** Changes in seasonal mean precipitation from 1981–2000 to 2061–2080.

(a, b, c) show results for winter and (d, e, f) results for summer. The first column (a, d) is the difference between the future and historical means for the CPM and the second column (b, e) is the same for the emulator, CPMGEM\_GCM. The third column (c, f) is the difference between the CPMGEM\_GCM and CPM changes. In all cases the differences are shown as percentages of the Historic CPM seasonal mean.

As well as an overall change in annual distribution, there are seasonal and spatial dependencies in the differences. It is projected that the UK will become drier in the summer and wetter in the winter (Kendon et al., 2021). Figure 10 shows the relative change in the mean precipitation between Historic and Future time periods for winter (top row; a, b, c) and summer (bottom row; d, e, f) for both the CPM (left column; a, d) and CPMGEM\_GCM (middle column; b, e). The right column (c, f) shows the difference between the mean changes in the CPM and in the emulator.

The emulator reproduces the mean drying in summer well. Summer is a particularly important season for the emulator to represent well, as a large component of UK summer rainfall is convective, and the UK CPM predicts changes in rainfall intensities that are substantially larger than in climate models with lower resolutions (Kendon et al., 2017). The emulator also captures most of the wettening in winter, though there is some underestimation. Table 2 shows the change in seasonal domain means. The change in summer is reproduced very accurately, but the winter change is underestimated by 26% relative to the change in the CPM (with 95% confidence interval 10–41% from boot-

Season	Percentile	CPM	Emulator
Winter	99	23.8	15.7 (12.4 to 17.8)
Winter	99.9	28.3	20.1 (16.8 to 24.1)
Summer	99	-7.0	-11.9 (-14.2 to -9.2)
Summer	99.9	12.5	1.5 (-1.0 to 5.6)

**Table 3. Percentage changes in heavy precipitation intensities (in %) between the Historic and Future time periods, for winter and summer.** Domain-mean of seasonal relative change in heavy daily-mean precipitation (99th and 99.9th percentile column 2) for CPM (column 3) and the CPMGEM\_GCM emulator (column 4). For the emulator, the value is the domain-mean of the percentage changes averaged over the 6 independent emulator sample runs (with the range across the samples given in brackets).

strapping, described in Section 2.4.3). The results indicate that the changes in spring (March–May, MAM) and autumn (September–November, SON) are also reproduced with the correct sign, but there is some evidence of underestimation and overestimation of the magnitude respectively. However, the magnitude of the mean changes in these seasons is relatively small, giving high sampling uncertainty of the relative differences, and their 95% confidence intervals overlap with zero. The values are similar for CPMGEM\_cCPM (see Table B1 in Appendix B).

To quantify future changes in the tail of the distribution of seasonal intensities, Table 3 shows percentage changes in heavy precipitation (99th and 99.9 percentiles) for winter and summer. As with the change in mean precipitation, the emulator successfully reproduces seasonal differences in future changes in heavy precipitation. It shows substantial increases in both of these percentiles in winter and in summer it correctly shows a decrease in the 99th and an increase in the 99.9th percentile. The different signs of the changes in summer are associated with decreases in rainfall frequency reducing moderate percentiles, but increases in the intensity of rainfall events dominating the more extreme percentiles. Results are similar for CPMGEM\_cCPM but with smaller error in the mean (Table B2).

However, in winter the emulator underestimates the future increases in these percentiles. In summer, the emulator’s changes are less positive than in the CPM, with the

decrease in the 99th percentile being overestimated and the increase in the 99.9th percentile underestimated. The change in these percentiles when using cCPM inputs is in better agreement with the CPM results (see Table B2), suggesting that part of the reason for the discrepancy in CPMGEM\_GCM’s predictions is differences between change signals in the GCM and coarsened CPM variables. However, the spread of predictions when using cCPM inputs still does not include the CPM changes in summer, indicating that the emulator did not fully learn the climate change signal in its training environment.

Changes in the frequency of wet and dry days are also critical to reproduce well. The emulator successfully reproduces the main features of seasonal differences in future changes in the frequency of wet days (precipitation greater than 0.1 mm). In winter, there is a small increase in wet days: a 2% relative increase in frequency versus a 5% increase in the CPM. In summer, a large decrease is predicted: a 38% decrease according to the emulator versus 36% in the CPM.

Overall, the emulator captures the main qualitative aspects of the climate change signal well, reproducing seasonal differences in precipitation changes as predicted by the CPM. However, there are quantitative errors in the emulator’s predictions of future changes. The emulator produces less positive increases in the mean precipitation in winter and in high percentiles in both winter and summer than the CPM. Some contribution to this comes from predicted changes in the frequency of precipitation being slightly smaller than in the CPM. But it also indicates that the emulator underestimates increases in the intensity of precipitation events.

### 3.4 Training with smaller datasets

We briefly discuss whether similar results could be obtained using CPM datasets of smaller size,  $\sim 10$ – $20$  years, corresponding to the amount of data available from some projects (e.g., Chan et al., 2020; Kendon et al., 2019), as opposed to the  $\sim 500$  years that we used to train the emulator discussed above. This is important for considering how widely the method could be applied. We train the low-data emulator CPMGEM<sub>ld</sub> on a much smaller dataset (14 years, one ensemble member in the Historic time period,  $\sim 3\%$  of the full training dataset size). We test it on the portion of the test dataset from the Historic time period and the same ensemble member as used for training (3 years). We



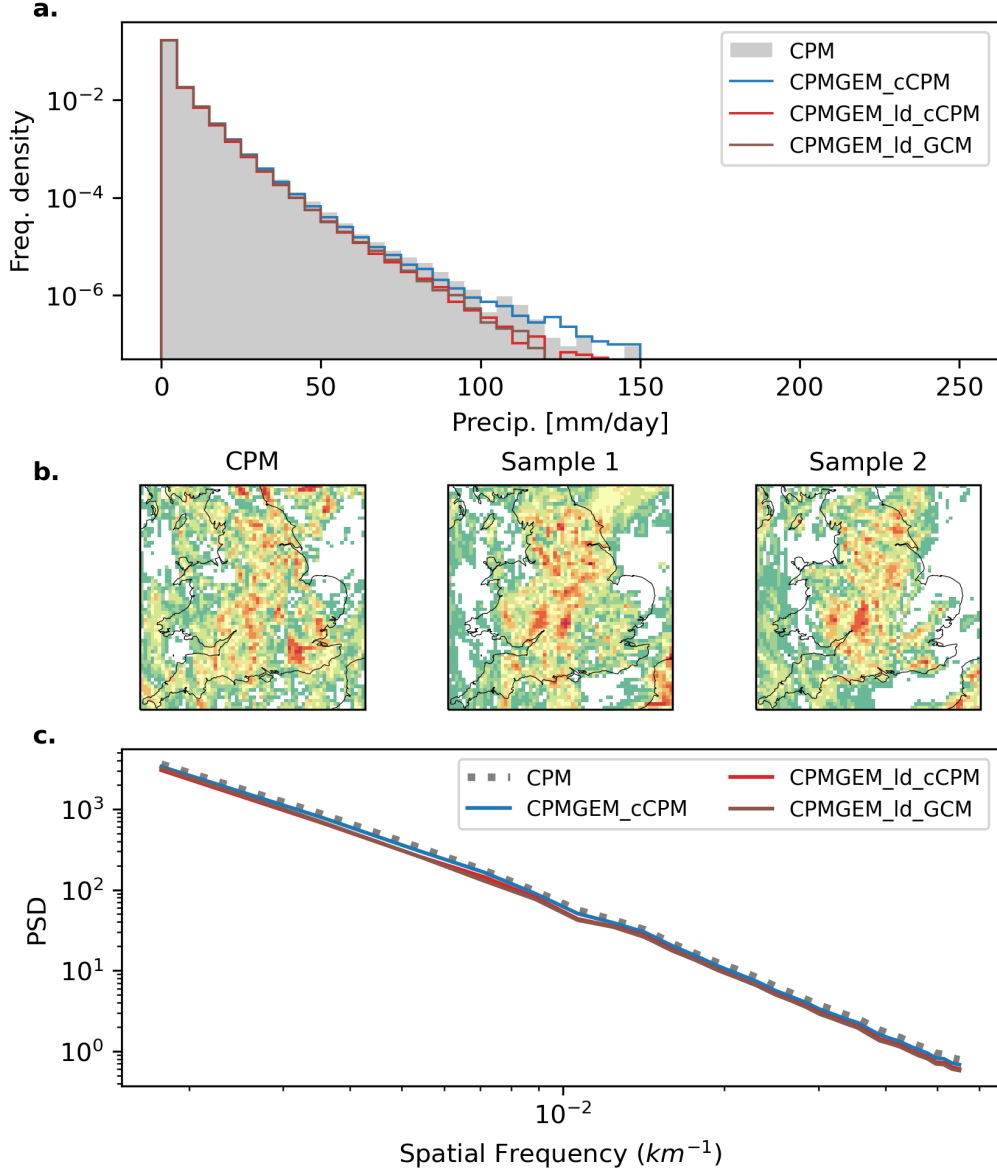


**Figure 11. Results for an emulator developed using a reduced (fourteen year) training dataset.** Both training and test data are from one ensemble member for the Historic time period only. (a) Histograms of precipitation values on the 8.8km grid: for the target CPM precipitation (grey filled area), the emulator developed using the full training data (CPMGEM\_cCPM, blue), and an emulator trained on the reduced data using coarsened CPM and GCM inputs: CPMGEM\_Id\_cCPM (purple) and CPMGEM\_Id\_GCM (dark green) respectively. Note the vertical axis is logarithmic. (b) Samples from the same “JJA Wet” day as in Figure 2, from the CPM (left) and two samples from CPMGEM\_Id\_cCPM (middle and right). (c) Radially-averaged spatial power spectral density (PSD) for the target CPM precipitation (grey dashed) and each emulator (colours as (a)).

find that, using either cCPM or GCM inputs, this emulator is able to recreate the frequency distribution of the CPM precipitation well (Figure 11(a)). Individual samples and the spatial power spectrum still appear realistic (Figure 11(b,c)).

Therefore the method does seem able to produce output matching the climatological CPM properties with this amount of data. The main challenge may be verification. With low amounts of high-resolution model data, it would be difficult to evaluate an emulator’s performance on rare, high-impact weather events, although there are methods that may assist (Watson, 2022). It would also be difficult to verify the emulated climate change signal, since there would be high sampling variability with such small amounts of data.

## 4 Discussion and conclusions

We have demonstrated results from CPMGEM, an emulator of a regional CPM based on a diffusion model, a generative machine learning method. It is able to produce samples of high-resolution (8.8km), daily-mean precipitation with realistic properties, conditional on coarse-resolution (60km) variables from the Met Office GCM. It has a much lower computational cost than the CPM. The output is at high enough space and time resolution for informing applications such as flood inundation modelling (e.g. Bates et al., 2023) and we have shown evidence that the emulator produces predictions with realistic structure and climatological frequency for extreme events with return times up to  $\sim 100$  years. The 21st century climate change signal is captured well in summer, the season when the CPM’s representation of convective processes is most valuable, but there is evidence of some error in the mean change in other seasons. We have used a  $\sim 500$  year training dataset for our main results, but also find that a good reproduction of climatological precipitation properties can also be obtained given only 14 years of training data.

The emulator is stochastic, and the stochastic component is reasonably well-calibrated, so that the emulator can create a range of plausible high-resolution samples for given large-scale conditions. From comparison to a deterministic U-Net model and other studies in the literature, the stochastic component is important for producing precipitation predictions with realistic small-scale structure and predicting the correct frequency of the most extreme intensities.

The main qualitative aspects of the 21st century climate change signal are captured well, including different patterns of change in summer compared to winter, and greater intensity increases for heavier events. The emulator captures well the mean change in summer, the season when the CPM’s representation of convective processes is most valuable. However, there is some error in the predicted magnitude of the changes in winter and in increases in heavy precipitation intensities in summer. A possible reason is that the climate change signal does not account for a large fraction of the variance of precipitation between randomly chosen days, so that the standard ML approach of optimising a skill score evaluated on each prediction independently does not provide a strong enough signal to improve the mean change. Therefore it may be valuable to develop modified training procedures that place more weight on capturing the climate change signal, such as using different loss functions. Including additional predictor variables may also give better performance. Development of methods to achieve a more faithful reproduction of the climate change signal whilst retaining the realistic spatial structure of samples would be highly valuable.

Further routes for development include increasing the output resolution and domain size in space and time yet further. Recently developed “video diffusion” methods could be applied to improve temporal coherence (e.g., Blattmann et al., 2023; Bar-Tal et al., 2024; Harvey et al., 2022), likely to be important for producing sub-daily predictions. Generating multi-variate output is another key target for climate impacts modelling. Further directions for evaluating the emulator include testing it with output from other GCMs, critical for application to augment available CPM simulations. Another evaluation approach would be to assess how realistic are the results if the emulator’s outputs are used to model impacts, such as flood inundation. Our results also indicate that improving generative ML methods so that they better capture the climate change signal would also be highly valuable.

## Open Research Section

The data for training and evaluating the models is available on Zenodo (Addison et al., 2025a). Trained model weights and samples from ML models are also available on Zenodo (Addison et al., 2025b). The code for this work is available on GitHub in 3 repositories and snapshots have been deposited on Zenodo: for processing the data (Addison, 2025b); for training and sampling from the ML models (Addison & Song, 2025); and for

evaluating the models (Addison, 2025a). In particular, the implementation of emulators (including full configuration) is developed on Github: <https://github.com/henryaddison/mlde>, which is a fork of [https://github.com/yang-song/score\\_sde\\_pytorch](https://github.com/yang-song/score_sde_pytorch) (Song et al., 2021). The configuration of our final CPMGEM emulator can be found in `ukcp_local_pr_12em_cnscnpp_continu`

## Acknowledgments

HA was supported by the UKRI Centre for Doctoral Training in Interactive Artificial Intelligence under Grant EP/S022937/1. EJK was supported by the Met Office Hadley Centre Climate Programme funded by DSIT under Grant GA01101. PAGW was supported by a Natural Environment Research Council Independent Research Fellowship (grant no. NE/S014713/1). We would like to thank Dr Stewart for compute resources used in the project, along with Bristol’s ACRC for maintaining the cluster.

## Author contributions:

- Conceptualization: HA, EJK, LA, PAGW
- Data curation: HA
- Formal Analysis: HA, LA, PAGW
- Methodology: HA, EJK, SR, LA, PAGW
- Investigation: HA, LA, PAGW
- Visualization: HA, LA, PAGW
- Resources: LA, PAGW
- Software: HA
- Supervision: EJK, SR, LA, PAGW
- Writing—original draft: HA, PAGW
- Writing—review & editing: HA, EJK, SR, LA, PAGW

**Competing interests:** The authors declare that they have no competing interests.

## References

- Addison, H. (2025a, March). *henryaddison/cpmgem-paper-evaluation*. Zenodo. Retrieved from <https://doi.org/10.5281/zenodo.15101996> doi: 10.5281/zenodo.15101996

- Addison, H. (2025b, March). *henryaddison/mlde-data: v0.3.0*. Zenodo. Retrieved from <https://doi.org/10.5281/zenodo.15102004> doi: 10.5281/zenodo.15102004
- Addison, H., Kendon, E., Ravuri, S., Aitchison, L., & Watson, P. (2025b, March). *Models and samples for ml emulators of met office uk cpm*. Zenodo. Retrieved from <https://doi.org/10.5281/zenodo.15097164> doi: 10.5281/zenodo.15097164
- Addison, H., Kendon, E., Ravuri, S., Aitchison, L., & Watson, P. A. (2025a, March). *Met office ukcp local cpm precipitation ml emulator dataset*. Zenodo. Retrieved from <https://doi.org/10.5281/zenodo.15096536> doi: 10.5281/zenodo.15096536
- Addison, H., Kendon, E. J., Ravuri, S., Aitchison, L., & Watson, P. (2022). Machine learning emulation of a local-scale uk climate model. In *Neurips 2022 workshop on tackling climate change with machine learning*. Retrieved from <https://www.climatechange.ai/papers/neurips2022/21>
- Addison, H., & Song, Y. (2025, March). *henryaddison/mlde: v0.2.1*. Zenodo. Retrieved from <https://doi.org/10.5281/zenodo.15101999> doi: 10.5281/zenodo.15101999
- Archer, L., Hatchard, S., Devitt, L., Neal, J. C., Coxon, G., Bates, P. D., ... Savage, J. (2024). Future change in urban flooding using new convection-permitting climate projections [Journal Article]. *Water Resources Research*, 60(1), e2023WR035533. Retrieved from <https://agupubs.onlinelibrary.wiley.com/doi/abs/10.1029/2023WR035533> doi: <https://doi.org/10.1029/2023WR035533>
- Bar-Tal, O., Chefer, H., Tov, O., Herrmann, C., Paiss, R., Zada, S., ... Michaeli, T. (2024). Lumiere: A space-time diffusion model for video generation [Journal Article]. *arXiv preprint arXiv:2401.12945*.
- Bates, P. D., Savage, J., Wing, O., Quinn, N., Sampson, C., Neal, J., & Smith, A. (2023). A climate-conditioned catastrophe risk model for uk flooding [Journal Article]. *Natural Hazards and Earth System Sciences*, 23(2), 891-908. Retrieved from <https://nhess.copernicus.org/articles/23/891/2023/> (NHES) doi: 10.5194/nhess-23-891-2023
- Blattmann, A., Rombach, R., Ling, H., Dockhorn, T., Kim, S. W., Fidler, S., &

- Kreis, K. (2023). Align your latents: High-resolution video synthesis with latent diffusion models [Conference Proceedings]. In *Proceedings of the IEEE/CVF conference on computer vision and pattern recognition* (p. 22563-22575).
- Boé, J., Mass, A., & Deman, J. (2022). A simple hybrid statistical–dynamical downscaling method for emulating regional climate models over western Europe. evaluation, application, and role of added value? [Journal Article]. *Climate Dynamics*, 61(1-2), 271-294. Retrieved from <https://doi.org/10.1007/s00382-022-06552-2> doi: 10.1007/s00382-022-06552-2
- Chan, S. C., Kendon, E. J., Berthou, S., Fosser, G., Lewis, E., & Fowler, H. J. (2020). Europe-wide precipitation projections at convection permitting scale with the unified model [Journal Article]. *Clim Dyn*, 55(3), 409-428. Retrieved from <https://www.ncbi.nlm.nih.gov/pubmed/32713994> doi: 10.1007/s00382-020-05192-8
- Chan, S. C., Kendon, E. J., Roberts, N., Blenkinsop, S., & Fowler, H. J. (2018). Large-scale predictors for extreme hourly precipitation events in convection-permitting climate simulations [Journal Article]. *Journal of Climate*, 31(6), 2115-2131. doi: 10.1175/Jcli-D-17-0404.1
- Dee, D. P., Uppala, S. M., Simmons, A. J., Berrisford, P., Poli, P., Kobayashi, S., ... Vitart, F. (2011). The era-interim reanalysis: configuration and performance of the data assimilation system [Journal Article]. *Quarterly Journal of the Royal Meteorological Society*, 137(656), 553-597. doi: 10.1002/qj.828
- Doury, A., Somot, S., & Gadat, S. (2024). On the suitability of a convolutional neural network based rcm-emulator for fine spatio-temporal precipitation [Journal Article]. *Climate Dynamics*, 62(9), 8587-8613. Retrieved from <GotoISI>://WOS:001277003700002 doi: 10.1007/s00382-024-07350-8
- Doury, A., Somot, S., Gadat, S., Ribes, A., & Corre, L. (2023). Regional climate model emulator based on deep learning: concept and first evaluation of a novel hybrid downscaling approach [Journal Article]. *Climate Dynamics*, 60(5-6), 1751-1779. Retrieved from <https://doi.org/10.1007/s00382-022-06343-9> doi: 10.1007/s00382-022-06343-9
- Efron, B. (1982). *The jackknife, the bootstrap and other resampling plans* [Book]. SIAM.
- Eyring, V., Bony, S., Meehl, G. A., Senior, C. A., Stevens, B., Stouffer, R. J., &

- Taylor, K. E. (2016). Overview of the coupled model intercomparison project phase 6 (cmip6) experimental design and organization [Journal Article]. *Geoscientific Model Development*, 9(5), 1937-1958. Retrieved from <https://gmd.copernicus.org/articles/9/1937/2016/> (GMD) doi: 10.5194/gmd-9-1937-2016
- Gutiérrez, J. M., Maraun, D., Widmann, M., Huth, R., Hertig, E., Benestad, R., ... Pagé, C. (2019). An intercomparison of a large ensemble of statistical downscaling methods over europe: Results from the value perfect predictor cross-validation experiment [Journal Article]. *International Journal of Climatology*, 39(9), 3750-3785. doi: 10.1002/joc.5462
- Harris, D., Foufoula-Georgiou, E., Droegemeier, K. K., & Levit, J. J. (2001). Multiscale statistical properties of a high-resolution precipitation forecast [Journal Article]. *Journal of Hydrometeorology*, 2(4), 406-418. doi: 10.1175/1525-7541(2001)002<0406:Mspoah>2.0.Co;2
- Harris, L., McRae, A. T. T., Chantry, M., Dueben, P. D., & Palmer, T. N. (2022). A generative deep learning approach to stochastic downscaling of precipitation forecasts [Journal Article]. *J Adv Model Earth Syst*, 14(10), e2022MS003120. Retrieved from <https://www.ncbi.nlm.nih.gov/pubmed/36590321> doi: 10.1029/2022MS003120
- Harvey, W., Naderiparizi, S., Masrani, V., Weillbach, C., & Wood, F. (2022). Flexible diffusion modeling of long videos [Conference Proceedings]. In (Vol. 35, p. 27953-27965).
- Haynes, K., Lagerquist, R., McGraw, M., Musgrave, K., & Ebert-Uphoff, I. (2023). Creating and evaluating uncertainty estimates with neural networks for environmental-science applications [Journal Article]. *Artificial Intelligence for the Earth Systems*, 2(2), 220061. Retrieved from <https://journals.ametsoc.org/view/journals/aies/2/2/AIES-D-22-0061.1.xml> doi: 10.1175/aies-d-22-0061.1
- Hess, P., Druke, M., Petri, S., Strnad, F. M., & Boers, N. (2022). Physically constrained generative adversarial networks for improving precipitation fields from earth system models [Journal Article]. *Nature Machine Intelligence*, 4(10), 828-839. doi: 10.1038/s42256-022-00540-1
- Ho, J., Jain, A., & Abbeel, P. (2020). Denoising diffusion probabilistic models [Con-

- ference Proceedings]. In *Advances in neural information processing systems* (Vol. 33, p. 6840-6851). Retrieved from <https://proceedings.neurips.cc/paper/2020/hash/4c5bcfec8584af0d967f1ab10179ca4b-Abstract.html>
- Jacob, D., Petersen, J., Eggert, B., Alias, A., Christensen, O. B., Bouwer, L. M., ... Yiou, P. (2014). Euro-cordex: new high-resolution climate change projections for european impact research [Journal Article]. *Regional Environmental Change*, 14(2), 563-578. doi: 10.1007/s10113-013-0499-2
- Kendon, E. J., Addison, H., Doury, A., Booth, B. B., Somot, S., Watson, P. A. G., ... Murphy, J. (2025). Potential for machine learning emulators to augment regional climate simulations in provision of local climate change information [Journal Article]. *Bulletin of the American Meteorological Society*.
- Kendon, E. J., Ban, N., Roberts, N. M., Fowler, H. J., Roberts, M. J., Chan, S. C., ... Wilkinson, J. M. (2017). Do convection-permitting regional climate models improve projections of future precipitation change? [Journal Article]. *Bulletin of the American Meteorological Society*, 98(1), 79-93. doi: 10.1175/bams-d-15-0004.1
- Kendon, E. J., Fischer, E. M., & Short, C. J. (2023). Variability conceals emerging trend in 100yr projections of uk local hourly rainfall extremes [Journal Article]. *Nat Commun*, 14(1), 1133. Retrieved from <https://www.ncbi.nlm.nih.gov/pubmed/36882408> doi: 10.1038/s41467-023-36499-9
- Kendon, E. J., Roberts, N. M., Fosser, G., Martin, G. M., Lock, A. P., Murphy, J. M., ... Tucker, S. O. (2020). Greater future u.k. winter precipitation increase in new convection-permitting scenarios [Journal Article]. *Journal of Climate*, 33(17), 7303-7318. Retrieved from <https://journals.ametsoc.org/view/journals/clim/33/17/jcliD200089.xml> doi: 10.1175/jcli-d-20-0089.1
- Kendon, E. J., Roberts, N. M., Fowler, H. J., Roberts, M. J., Chan, S. C., & Senior, C. A. (2014). Heavier summer downpours with climate change revealed by weather forecast resolution model [Journal Article]. *Nature Climate Change*, 4(7), 570-576. Retrieved from <https://doi.org/10.1038/nclimate2258> doi: 10.1038/nclimate2258
- Kendon, E. J., Roberts, N. M., Senior, C. A., & Roberts, M. J. (2012). Realism of rainfall in a very high-resolution regional climate model [Journal Article]. *Journal of Climate*, 25(17), 5791-5806. Retrieved from



- <GotoISI>://WOS:000308633500010 doi: 10.1175/Jcli-D-11-00562.1
- Kendon, E. J., Short, C., Pope, J., Chan, S., Wilkinson, J., Tucker, S., ... Harris, G. (2021). *Update to ukcp local (2.2km) projections* (Journal Article). Retrieved from [https://www.metoffice.gov.uk/pub/data/weather/uk/ukcp18/science-reports/ukcp18\\_local\\_update\\_report\\_2021.pdf](https://www.metoffice.gov.uk/pub/data/weather/uk/ukcp18/science-reports/ukcp18_local_update_report_2021.pdf)
- Kendon, E. J., Stratton, R. A., Tucker, S., Marsham, J. H., Berthou, S., Rowell, D. P., & Senior, C. A. (2019). Enhanced future changes in wet and dry extremes over africa at convection-permitting scale [Journal Article]. *Nat Commun*, 10(1), 1794. Retrieved from <https://www.ncbi.nlm.nih.gov/pubmed/31015416> doi: 10.1038/s41467-019-09776-9
- Klaver, R., Haarsma, R., Vidale, P. L., & Hazeleger, W. (2020). Effective resolution in high resolution global atmospheric models for climate studies [Journal Article]. *Atmospheric Science Letters*, 21(4), e952. doi: 10.1002/asl.952
- Leach, N. J., Watson, P. A. G., Sparrow, S. N., Wallom, D. C. H., & Sexton, D. M. H. (2022). Generating samples of extreme winters to support climate adaptation [Journal Article]. *Weather and Climate Extremes*, 36, 100419. Retrieved from <https://www.sciencedirect.com/science/article/pii/S2212094722000111> doi: 10.1016/j.wace.2022.100419
- Leinonen, J., Nerini, D., & Berne, A. (2020). Stochastic super-resolution for downscaling time-evolving atmospheric fields with a generative adversarial network [Journal Article]. *IEEE Transactions on Geoscience and Remote Sensing*, 1–13.
- Leutbecher, M., & Palmer, T. N. (2008). Ensemble forecasting [Journal Article]. *Journal of Computational Physics*, 227(7), 3515–3539. Retrieved from <https://www.sciencedirect.com/science/article/pii/S0021999107000812> doi: 10.1016/j.jcp.2007.02.014
- Maher, N., Milinski, S., & Ludwig, R. (2021). Large ensemble climate model simulations: introduction, overview, and future prospects for utilising multiple types of large ensemble [Journal Article]. *Earth System Dynamics*, 12(2), 401–418.
- Maraun, D., Shepherd, T. G., Widmann, M., Zappa, G., Walton, D., Gutiérrez, J. M., ... Mearns, L. O. (2017). Towards process-informed bias correction of climate change simulations [Journal Article]. *Nature Climate Change*, 7(11), 764–773. doi: 10.1038/nclimate3418

- Maraun, D., & Widmann, M. (2018). *Statistical downscaling and bias correction for climate research* [Book]. Cambridge University Press.
- Maraun, D., Widmann, M., & Gutierrez, J. M. (2019). Statistical downscaling skill under present climate conditions: A synthesis of the value perfect predictor experiment [Journal Article]. *International Journal of Climatology*, 39(9), 3692-3703. doi: 10.1002/joc.5877
- Mardani, M., Brenowitz, N., Cohen, Y., Pathak, J., Chen, C.-Y., Liu, C.-C., ... Pritchard, M. (2023). Residual diffusion modeling for km-scale atmospheric downscaling [Journal Article]. *arXiv preprint arXiv:2309.15214*.
- Murphy, J., Harris, G., Sexton, D., Kendon, E., Bett, P., Clark, R., ... Lowe, J. (2018). *Ukcp18 land projections: science report* (Journal Article). Retrieved from <https://www.metoffice.gov.uk/pub/data/weather/uk/ukcp18/science-reports/UKCP18-Land-report.pdf>
- Ravuri, S., Lenc, K., Willson, M., Kangin, D., Lam, R., Mirowski, P., ... Mohamed, S. (2021). Skilful precipitation nowcasting using deep generative models of radar [Journal Article]. *Nature*, 597(7878), 672-677. doi: 10.1038/s41586-021-03854-z
- Ronneberger, O., Fischer, P., & Brox, T. (2015). U-net: Convolutional networks for biomedical image segmentation [Journal Article]. *Medical Image Computing and Computer-Assisted Intervention, Pt Iii*, 9351, 234-241. doi: 10.1007/978-3-319-24574-4\_28
- Schaller, N., Sillmann, J., Muller, M., Haarsma, R., Hazeleger, W., Hegdahl, T. J., ... Whan, K. (2020). The role of spatial and temporal model resolution in a flood event storyline approach in western norway [Journal Article]. *Weather and Climate Extremes*, 29, 100259. doi: 10.1016/j.wace.2020.100259
- Schoof, J. T. (2013). Statistical downscaling in climatology [Journal Article]. *Geography Compass*, 7(4), 249-265. Retrieved from <https://compass.onlinelibrary.wiley.com/doi/abs/10.1111/gec3.12036> doi: 10.1111/gec3.12036
- Schultz, M. G., Betancourt, C., Gong, B., Kleinert, F., Langguth, M., Leufen, L. H., ... Stadler, S. (2021). Can deep learning beat numerical weather prediction? [Journal Article]. *Philosophical Transactions of the Royal Society A: Mathematical, Physical and Engineering Sciences*, 379(2194), 20200097. doi:

10.1098/rsta.2020.0097

- Sha, Y. K., Gagne, D. J., West, G., & Stull, R. (2020). Deep-learning-based gridded downscaling of surface meteorological variables in complex terrain. part ii: Daily precipitation [Journal Article]. *Journal of Applied Meteorology and Climatology*, 59(12), 2075-2092. doi: 10.1175/Jamc-D-20-0058.1
- Sinclair, S., & Pegram, G. G. S. (2005). Empirical mode decomposition in 2-d space and time: a tool for space-time rainfall analysis and nowcasting [Journal Article]. *Hydrology and Earth System Sciences*, 9(3), 127-137. doi: DOI10.5194/hess-9-127-2005
- Sobolowski, S., Somot, S., Fernandez, J., Evin, G., Maraun, D., Kotlarski, S., ... Brands, S. (2023, February). *EURO-CORDEX CMIP6 GCM Selection & Ensemble Design: Best Practices and Recommendations*. Zenodo. Retrieved from <https://doi.org/10.5281/zenodo.7673400> doi: 10.5281/zenodo.7673400
- Sohl-Dickstein, J., Weiss, E., Maheswaranathan, N., & Ganguli, S. (2015). Deep unsupervised learning using nonequilibrium thermodynamics [Conference Proceedings]. In *International conference on machine learning* (p. 2256-2265). PMLR.
- Song, Y., & Ermon, S. (n.d.). Generative modeling by estimating gradients of the data distribution [Conference Proceedings]. In *Advances in neural information processing systems* (Vol. 32). Retrieved from <https://proceedings.neurips.cc/paper/2019/hash/3001ef257407d5a371a96dcd947c7d93-Abstract.html>
- Song, Y., Sohl-Dickstein, J., Diederik, Kumar, A., Ermon, S., & Poole, B. (2021). Score-based generative modeling through stochastic differential equations [Conference Proceedings]. In *Iclr*. doi: arxiv:2011.13456
- Vandal, T., Kodra, E., & Ganguly, A. R. (2018). Intercomparison of machine learning methods for statistical downscaling: the case of daily and extreme precipitation [Journal Article]. *Theoretical and Applied Climatology*, 137(1-2), 557-570. doi: 10.1007/s00704-018-2613-3
- van der Meer, M., de Roda Husman, S., & Lhermitte, S. (2023). Deep learning regional climate model emulators: A comparison of two downscaling training frameworks [Journal Article]. *Journal of Advances in Modeling Earth Systems*, 15(6), e2022MS003593. doi: 10.1029/2022ms003593

- Vosper, E., Watson, P., Harris, L., McRae, A., Santos-Rodriguez, R., Aitchison, L., & Mitchell, D. (2023). Deep learning for downscaling tropical cyclone rainfall to hazard-relevant spatial scales [Journal Article]. *Journal of Geophysical Research-Atmospheres*, 128(10), e2022JD038163. doi: 10.1029/2022JD038163
- Walton, D. B., Sun, F. P., Hall, A., & Capps, S. (2015). A hybrid dynamical-statistical downscaling technique. part i: Development and validation of the technique [Journal Article]. *Journal of Climate*, 28(12), 4597-4617. doi: 10.1175/Jcli-D-14-00196.1
- Wang, F., Tian, D., & Carroll, M. (2023). Customized deep learning for precipitation bias correction and downscaling [Journal Article]. *Geoscientific Model Development*, 16(2), 535-556. Retrieved from <https://gmd.copernicus.org/articles/16/535/2023/> (GMD) doi: 10.5194/gmd-16-535-2023
- Watson, P. A. G. (2022). Machine learning applications for weather and climate need greater focus on extremes [Journal Article]. *Environmental Research Letters*, 17(11), 111004. Retrieved from <https://dx.doi.org/10.1088/1748-9326/ac9d4e> doi: 10.1088/1748-9326/ac9d4e
- Watson, P. A. G. (2023). Machine learning applications for weather and climate predictions need greater focus on extremes: 2023 update. In *Neurips 2023 workshop on tackling climate change with machine learning*. Retrieved from <https://www.climatechange.ai/papers/neurips2023/29>
- Weaver, C. P., Moss, R. H., Ebi, K. L., Gleick, P. H., Stern, P. C., Tebaldi, C., ... Arvai, J. L. (2017, jul). Reframing climate change assessments around risk: recommendations for the us national climate assessment. *Environmental Research Letters*, 12(8), 080201. Retrieved from <https://dx.doi.org/10.1088/1748-9326/aa7494> doi: 10.1088/1748-9326/aa7494
- Widmann, M., Bedia, J., Gutierrez, J. M., Bosshard, T., Hertig, E., Maraun, D., ... Huth, R. (2019). Validation of spatial variability in downscaling results from the value perfect predictor experiment [Journal Article]. *International Journal of Climatology*, 39(9), 3819-3845. doi: 10.1002/joc.6024

## Appendix A Diffusion models

Probabilistic models assume that observed data, such as high-resolution precipitation over the UK, is drawn from an unknown distribution  $p^*(\mathbf{x})$ . A conditional model such as our high-resolution precipitation emulator conditioned on coarse inputs  $p^*(\mathbf{x}|\mathbf{y})$  can also be considered but for simplicity we will stick with the unconditional version.

Song et al. (2021) combine earlier approaches (Song & Ermon, n.d.; Ho et al., 2020) into a single framework called Score-Based Generative Models with Stochastic Differential Equations (SDE). The idea is to imagine a diffusion process  $\{\mathbf{x}(t)_{t=0}^T\}$  modelled by an SDE:

$$d\mathbf{x} = \mathbf{f}(\mathbf{x}, t)dt + g(t)d\mathbf{w} \quad (\text{A1})$$

When run forward, a sample,  $\mathbf{x}(0)$ , from the data distribution,  $p_0$ , is gradually perturbed over time into a sample from a final noise distribution,  $p_T$ . The final distribution is chosen as something tractable for sampling, usually a Gaussian.

More interesting for us is running the reverse diffusion process:

$$d\mathbf{x} = [\mathbf{f}(\mathbf{x}, t) - g(t)^2 \nabla_{\mathbf{x}} \log p_t(x)]dt + g(t)d\bar{\mathbf{w}} \quad (\text{A2})$$

By solving this, samples from  $p_T$  (which are easy to produce by design) can be converted into samples from the original data distribution. This requires two steps: calculating the score,  $\nabla_{\mathbf{x}} \log p_t(x)$ , and then applying numerical approaches to solve Equation A2.

The score is estimated as a neural net  $s_\theta(\mathbf{x}, t)$  where  $\theta$  are determined by minimizing:

$$\mathbb{E}_t \{ \lambda(t) \mathbb{E}_{\mathbf{x}(0)} \mathbb{E}_{\mathbf{x}(0)|\mathbf{x}(t)} [ \|s_\theta(\mathbf{x}(t), t) - \nabla_{\mathbf{x}(t)} \log p_{0t}(\mathbf{x}(t)|\mathbf{x}(0))\|_2^2 ] \} \quad (\text{A3})$$

where  $\lambda$  is a positive weighting function that is chosen along with  $\mathbf{f}$  and  $\mathbf{g}$ .

Song et al. (2021) summarize three approaches for solving the reverse SDE. General-purpose numerical methods can be used to find approximate solutions to the SDE. Predictor-Corrector sampling takes this a step further by using making use of estimated score at

each timestep to apply a correction to the sample estimated at that timestep by the general purpose solver. Alternatively the problem can be reformulated as a deterministic process without affecting the trajectory probabilities and in turn solved using an ODE solver.

## Appendix B Further climate change results

Table B1 and Table B2 show climate change related results based on cCPM inputs rather than GCM inputs as used in the main text.

Season	CPM (%)	Emulator (%)	Difference (% of CPM change)	Difference (% of Historic CPM)
DJF	23	18	-21 (-33 to -9)	-6 (-7.7 to -2.0)
MAM	6	4	-31 (-78 to +16)	-2 (-4.8 to +1.0)
JJA	-40	-39	2 (-7 to +10)	1 (-2.9 to +3.9)
SON	-4	-6	-59 (-129 to +9)	-2 (-5.1 to +0.4)

**Table B1. Change in seasonal domain mean for CPMGEM\_cCPM.** As Table 2 for

CPMGEM\_cCPM. Shows changes in the domain mean from Historic to Future periods for each season. The second and third columns contain the relative changes for the CPM and the CPMGEM\_cCPM emulator respectively (relative to CPM Historic seasonal domain mean in both cases). The fourth column contains the difference between the change in the CPM and CPMGEM\_cCPM, relative to the change in CPM. The fifth column shows the same difference but relative to the Historic CPM seasonal domain mean. The values in brackets in these columns are the bootstrapped 95% confidence intervals of the difference.

Season	Percentile	CPM	Emulator
Winter	99	23.8	18.7 (15.3 to 24.6)
Winter	99.9	28.3	25.0 (20.6 to 31.0)
Summer	99	-7.0	-10.9 (-12.3 to -9.5)
Summer	99.9	12.5	9.9 (9.3 to 11.3)

**Table B2. Percentage changes in heavy precipitation intensities (in %) between the Historic and Future time periods, for winter and summer using CPMGEM\_cCPM predictions.** As in Table 3 for CPMGEM\_cCPM. Domain-mean of seasonal relative change in heavy daily-mean precipitation (99th and 99.9th percentile column 2) for CPM (column 3) and the CPMGEM\_cCPM emulator (column 4). For the emulator, the value is the domain-mean of the percentage changes averaged over the 6 independent emulator sample runs (with the range across the samples given in brackets).